

Nonperturbative Resummation of Divergent Time-Local Generators

Dragomir Davidovic^{1,*}

¹*School of Physics, Georgia Institute of Technology, USA*

(Dated:)

Time-local generators of open quantum systems are generically divergent at long times, even though the reduced dynamics remains regular. We construct, by analytic continuation, nonperturbative dynamical maps consistent with these generators. For the weak-coupling unbiased spin-boson model, this construction yields an explicit dynamical map that nonperturbatively resums the TCL generator and exposes how the divergences signal the approach to a singular time at which the reduced dynamics becomes noninvertible. The reconstructed map is validated against TEMPO simulations at short times and the exactly solvable rotating-wave model at all times. In the full spin-boson model, the same continuum mechanism produces both an early-time anisotropy, with a measurable phase shift that provides a signature of the environmental correlation and the pointer direction, and a late-time singularity at which the reduced dynamics becomes noninvertible. By contrast, in the rotating-wave model the map approaches this point without reaching it and remains invertible at all times. These results establish a nonperturbative framework for reconstructing reduced dynamics from divergent time-local generators, diagnosing the onset of noninvertibility, and identifying experimentally accessible early-time signatures of environment-induced anisotropy.

I. INTRODUCTION

Reduced open quantum system evolution is described by a completely positive trace-preserving (CPTP) dynamical map $\Phi(t)$ acting on the density matrix [1]. A time-local master equation represents the same evolution through a generator $L(t)$ defined by

$$L(t) = \dot{\Phi}(t)\Phi^{-1}(t). \quad (1)$$

Thus the time-local generator is the logarithmic derivative of the dynamical map and exists only while the map remains invertible.

Formally, time-local master equations are derived from the time-convolutionless projection-operator expansion [2]. This provides one of two exact projection-operator representations of reduced dynamics, the other being the Nakajima-Zwanzig memory-kernel equation [1].

In a cumulant expansion for stochastic linear differential equations, the time-local generator is obtained through the cumulant (van Kampen) resummation derived from the Feynman disentanglement theorem [3, 4]. In this method, $\Phi(t)$ is reorganized into an exponential of cumulants $K_n(t)$ that encode progressively higher-order system-bath interactions. A remarkable feature of this construction is that it remains valid in the genuinely quantum regime, where interaction operators at different times do not commute. When bath correlations decay sufficiently rapidly, the expansion removes the secular growth present in the Dyson series order by order.

However, when environmental correlations decay slowly, the cumulant expansion generically diverges at long time scales, with divergences appearing already at

fourth order [5] and not removed by resummation of the leading cumulants [6]. This occurs even though the underlying propagator remains well defined, consistent with convergence of the Dyson expansion [7].

Rather than signaling a breakdown of the reduced dynamics, the divergence reflects the approach to a rank change of the dynamical map. A singular value vanishes and the corresponding time-local generator becomes unbounded [Eq. (1)]. It therefore signals the approach to a noninvertible quantum channel, as illustrated by the Schrödinger-cat example in Fig. 1. Once the singular time is crossed, the reduced dynamics no longer retains enough information to resurrect the initial superposition.

To show that noninvertibility indeed occurs, we exploit the fact that the resummed cumulant expansion remains well defined at early time scales. Its controlled growth at early times carries signatures of both an impending singularity and an experimentally accessible anisotropy in the coherence dynamics. We use this early-time behavior to define an analytic continuation of the reduced dynamics. The map is then reconstructed using the Feynman disentanglement theorem, with the Davies reference semigroup serving as the anchor of the continuation. The generator is then recovered, with its singular structure made explicit through the logarithmic derivative of the reconstructed map, Eq. (1).

The main conceptual result of this paper then follows: in continuum environments with slowly decaying correlations, the same continuum mechanism produces two distinct effects. At early times it generates an anisotropy in the nonsecular coherence transfer, with a measurable phase shift that carries information about the environmental correlation and the pointer direction. At late times, the dynamical map reaches rank deficiency at finite time. The present method reveals the microscopic origin of both effects. It lies in the coupling between nonsecular coherence dynamics and the pole-branch structure of the bath correlation function [8]. After the Marko-

* dragomir.davidovic@physics.gatech.edu

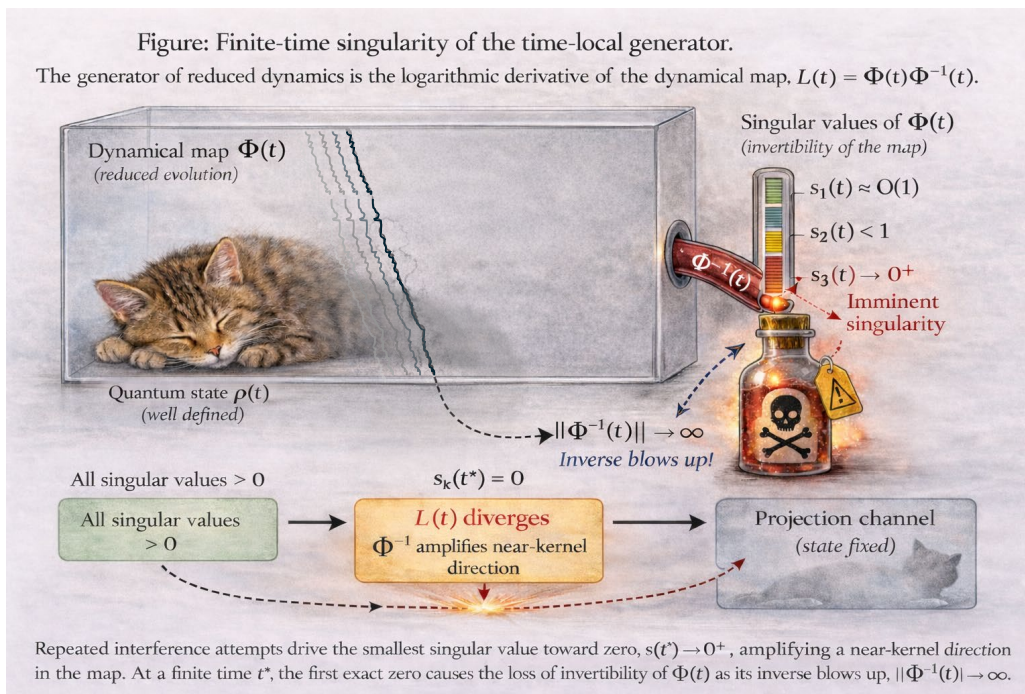


FIG. 1. Finite-time loss of invertibility of the dynamical map induced by system–environment interactions. Markovian relaxation, nonsecular coherence mixing, and the Khalfin tail jointly drive the smallest singular value toward zero. The repeated crack-like features reflect successive destructive interference between the exponential contribution and the bath correlation function, progressively suppressing coherence. At the final crack, a singular value vanishes, marking noninvertibility. Beyond this point, resurrection of the initial superposition from the reduced dynamics is no longer possible.

vian decay has been completed and the dynamics crosses over to the nonexponential decay law [9], the secular and nonsecular coherence contributions acquire a common asymptotic tail but cross over to that tail at parametrically different times. The same continuum structure that produces an early observable anisotropy ultimately drives the loss of invertibility.

As a concrete illustration, we apply the method to the weak-coupling unbiased spin–boson model and show how the reconstructed dynamics exhibits both an early-time anisotropy in the coherence transfer and a finite-time loss of invertibility. A useful benchmark is provided by the exactly solvable rotating-wave approximation (RWA) model. In this case, the reduced dynamical map comes very close to the same singular point but does not reach it because of the residual phase mismatch. The RWA dynamics therefore remains invertible, even though it exhibits the same late-time nonexponential decay law.

Beyond its role in revealing the singular structure of the generator, the present method offers a practical computational advantage. The disentanglement procedure effectively separates the environmental modes, so their resummed influence enters polynomially through bath correlation functions rather than via multiplicative Hilbert-space embeddings. As discussed in Sec. III, the exponential complexity associated with Hilbert-space enlargement—or with influence-functional approaches—is replaced by polynomial scaling, establishing a fundamen-

tally different computational strategy for open-system dynamics.

A further point concerns the regime of applicability of the method. The present approach relies on invertible maps to diagnose the onset of noninvertibility. This is justified by the density of invertible CPTP maps in the set of all CPTP maps. Any noninvertible channel can be obtained as a limit of invertible channels with arbitrarily small but nonzero coherences or populations in the discarded subspace.

In actual calculations, the reconstructed map is obtained from a truncated or partially resummed cumulant expansion. Such approximations can exhibit spurious behavior near the singular point: the smallest singular value may reach zero and subsequently increase, artificially restoring invertibility. Physically, the vanishing of a singular value marks loss of invertibility and the associated collapse of distinguishability along a direction in state space. Any apparent restoration of invertibility would therefore require passage through a non-CPTP regime, as shown in Sec. VIII A. We therefore identify the onset of noninvertibility with the first zero of the smallest singular value and restrict the reconstructed map to times up to this point.

We now position the present approach relative to previous treatments of time-local generators. In regimes where the dynamical map remains invertible and the generator stays regular, a number of complementary con-

structions are available. Explicit dilations exist for certain time-local quantum Markov processes [10], operator-algebra methods can derive generators directly from microscopic dynamics in specific settings [11], and related work seeks Lindblad generators consistent with conservation laws and thermalization for systems weakly coupled to baths [12]. Related exact examples also occur in solvable models, including linearly coupled harmonic systems interacting with a harmonic bath [13], where the Gaussian structure allows the dynamical map to be written explicitly, as well as excitation-conserving Hamiltonians such as the RWA, where the reduced dynamics can be solved analytically [14].

A different situation arises for continuum environments with slowly decaying bath correlations, where late-time divergences of time-local generators were first obtained analytically in special infrared regimes within a fourth-order TCL expansion [5], and were later shown to be generic rather than infrared-specific [6]. Analyses of higher-order TCL dynamics in specific models further show that late-time non-Markovianity is regime dependent and may either increase or decrease at long times [15]. Existing strategies typically address these difficulties by modifying the generator itself, for example through pseudoinverse constructions [16], effective-field-theory resummations [17], or by enforcing complete positivity via projection onto the nearest CPTP map [18].

The present work takes a complementary viewpoint. Starting from a generator that becomes singular at long times, we do not attempt to regularize the singularity. Instead, we analytically continue the dynamical map obtained from the generator and interpret the singular behavior.

Outline. The remainder of the paper develops the dynamical-map reconstruction and its physical interpretation. We first formulate the reduced-dynamics framework and introduce the disentangled representation based on a time-local generator. We then analyze the reconstructed singularities in a rotating-wave benchmark, and finally apply the method to the full spin-boson dynamics.

II. THE STANDARD OPEN SYSTEM SETUP

We consider a finite-level quantum system weakly coupled to a bosonic environment. The total Hamiltonian is

$$H_T = H_S + H_B + H_I. \quad (2)$$

The system Hamiltonian is diagonal in its energy eigenbasis,

$$H_S = \sum_{n=1}^N E_n |n\rangle\langle n|, \quad (3)$$

with Bohr frequencies $\omega_{nm} = E_n - E_m$. The environment

consists of baths of harmonic modes

$$H_B = \sum_{k,\alpha} \omega_{k,\alpha} b_{k,\alpha}^\dagger b_{k,\alpha}, \quad (4)$$

where α and k denote the bath and mode indices, respectively. Different baths are assumed to be uncorrelated, and the coupling is taken in separable form

$$H_I = \sum_{\alpha} A^{\alpha} \otimes F_{\alpha}, \quad (5)$$

where A^{α} is a dimensionless Hermitian system operator that couples the system to bath α , normalized to have operator norm of order unity and

$$F_{\alpha} = \sum_k g_{k,\alpha} (b_{k,\alpha} + b_{k,\alpha}^\dagger) \quad (6)$$

is a Hermitian bath operator with coupling constants $g_{k,\alpha} \propto \lambda \ll 1$.

Bath correlations

The reduced dynamics are governed by the bath correlation function

$$C_{\alpha}(t) = \langle F_{\alpha}(t) F_{\alpha}(0) \rangle_{\beta}, \quad (7)$$

defined with respect to a thermal equilibrium state at inverse temperature β . The bath is characterized by the spectral density

$$\tilde{J}_{\omega}^{\alpha} = \pi \sum_k g_{k,\alpha}^2 \delta(\omega - \omega_{k,\alpha}), \quad \omega > 0, \quad (8)$$

where the tilde denotes zero temperature. We employ the canonical continuum environments used in the spin-boson model [19],

$$\tilde{J}_{\omega}^{\alpha} = 2\pi\lambda^2 \frac{\omega^s}{\omega_c^{s-1}} e^{-\omega/\omega_c} \Theta(\omega), \quad (9)$$

where ω_c is the ultraviolet cutoff frequency and s is the spectral exponent (Ohmic $s = 1$, sub-Ohmic $0 < s < 1$, super-Ohmic $s > 1$).

The thermal spectral density is

$$J_{\omega}^{\alpha} = \frac{\tilde{J}_{\omega}^{\alpha}}{1 - e^{-\beta\omega}}, \quad \omega > 0, \quad (10)$$

with the extension to negative frequencies fixed by detailed balance,

$$J_{-\omega}^{\alpha} = e^{-\beta\omega} J_{\omega}^{\alpha}. \quad (11)$$

The bath correlation function admits the Fourier representation

$$C_{\alpha}(t) = \frac{1}{\pi} \int_{-\infty}^{\infty} d\omega J_{\omega}^{\alpha} e^{-i\omega t}, \quad (12)$$

which at zero temperature reduces to

$$\tilde{C}_{\alpha}(t) = \frac{2\lambda^2\omega_c^2\Gamma(s+1)}{(1+i\omega_c t)^{s+1}}. \quad (13)$$

Half-sided transform

A central quantity is the half-sided Fourier transform

$$\Gamma_\omega^\alpha = \int_0^\infty dt C_\alpha(t) e^{i\omega t} = J_\omega^\alpha + iS_\omega^\alpha, \quad (14)$$

which is analytic for $\text{Im } \omega > 0$. Its finite-time counterpart defines the memory kernel

$$\Gamma_\omega^\alpha(t) = \int_0^t d\tau C_\alpha(\tau) e^{i\omega\tau}, \quad (15)$$

which is entire in ω and converges to Γ_ω^α as $t \rightarrow \infty$.

Assumptions

The analysis assumes a controlled weak-coupling open-system limit with well separated dynamical scales.

1. *Weak coupling.*

$$\lambda^2 \ll 1,$$

which is necessary for the Davies generator L_0 to provide the leading reduced dynamics.

2. *Resolved system frequencies.* The bath-induced relaxation rate remains small compared with the Bohr frequencies,

$$\gamma \sim J(\omega_{nm}) \ll |\omega_{nm}|.$$

which in the spin-boson model reduces to $\gamma \ll \Delta$.

These scale separations are the necessary and sufficient conditions underlying the van Hove weak-coupling limit and ensure the existence of a well-defined pole contribution to the dynamics.

3. *Continuum environment.* The bath is taken in the thermodynamic limit with a continuous spectral density (9) and finite cutoff ω_c , producing long-time branch-cut contributions responsible for non-exponential (Khalfin) decay.
4. *Separated timescales.* There exists an intermediate time window

$$T_1, T_2 \ll t \ll t_{\text{rec}},$$

with relaxation times $T_{1,2}$ and recurrence time t_{rec} . The reconstruction and interpretation of generator singularities apply in this regime.

These conditions define the parameter domain in which divergences of the time-local generator are interpreted.

III. TIME-LOCAL GENERATOR

To uncover the structure of the divergent generator, we first examine the cumulant (van Kampen) expansion. In this formulation the propagator can be written as a time-ordered exponential,

$$\Phi(t) = \mathcal{T} \exp \left[\int_0^t d\tau L(\tau) \right], \quad L(t) = \sum_{n=0}^{\infty} L_n(t), \quad (16)$$

where the cumulants $L_n(t)$ encode progressively higher-order system-bath interactions [3, 4]. Each cumulant effectively resums an infinite subset of Dyson terms, so that resumming the cumulant hierarchy amounts to a nested resummation of the Dyson expansion.

The behavior of this expansion in slowly decaying environments was analyzed in Ref. [6]. That work showed that resummation of the leading cumulants generates conjugate pairs of modes, one exponentially decaying and the other exponentially growing. This pairing follows from the antisymmetry of the renormalized transition frequencies inherited from the Bohr spectrum. As a result, the bath-induced imaginary parts enter with opposite signs for the two paired transitions: if one mode acquires a positive decay rate, its conjugate necessarily acquires the opposite rate. When environmental memory cannot suppress the growing component, the cumulant expansion diverges and the corresponding time-local generator becomes unbounded.

Building on Ref. [6], we construct a partially resummed TCL generator and extend the result to the case of multiple uncorrelated baths,

$$L(t) = -i[H_S, \cdot] + K(t), \quad (17)$$

with the resummed dissipator

$$\begin{aligned} K_{nm,ij}(t) = & \sum_{\alpha} A_{ni}^{\alpha} A_{jm}^{\alpha} \left[\Gamma_{\omega_{in}^{(j)}}^{\alpha}(t)(t) + [\Gamma_{\omega_{jm}^{(i)}}^{\alpha}(t)(t)]^{\star} \right] \\ & - \sum_{\alpha, k} \left[\delta_{jm} A_{nk}^{\alpha} A_{ki}^{\alpha} \Gamma_{\omega_{ik}^{(j)}}^{\alpha}(t)(t) \right. \\ & \left. + \delta_{ni} A_{jk}^{\alpha} A_{km}^{\alpha} [\Gamma_{\omega_{jk}^{(i)}}^{\alpha}(t)(t)]^{\star} \right], \end{aligned} \quad (18)$$

where the renormalized complex frequencies are

$$\begin{aligned} \omega_{in}^{(j)}(t) = & \omega_{in} - i \left[\sum_{c, \alpha} \left(|A_{ic}^{\alpha}|^2 \Gamma_{\omega_{ic}}^{\alpha}(t) - |A_{nc}^{\alpha}|^2 \Gamma_{\omega_{nc}}^{\alpha}(t) \right) \right. \\ & \left. + \sum_{\alpha} 2J_0^{\alpha}(t) A_{jj}^{\alpha} (A_{nn}^{\alpha} - A_{ii}^{\alpha}) \right]. \end{aligned} \quad (19)$$

The first term is the Fermi-Golden-Rule contribution, while the second term $\Omega_{jni}^{\alpha}(t) = 2J_0^{\alpha}(t) A_{jj}^{\alpha} (A_{nn}^{\alpha} - A_{ii}^{\alpha})$ is the spectral-overlap correction due to bath α , that couples populations and coherences beyond Born-Markov theory. For reference, and to clarify these expressions, the explicit matrix elements for the spin-boson model coupled to a single bath are given in Appendix A.

The time-local generator, Eq. (18), has a Redfield-type superoperator form. This does not imply a second-order perturbative approximation. For a bilinear system–environment interaction $H_I = A \otimes B$, eliminating the environmental degrees of freedom produces superoperators composed of combinations of $A\rho$ and ρA (as well as related operators) at all perturbative orders. The appearance of a Redfield-like tensor therefore follows from the structure of the interaction Hamiltonian and from the selection of the leading cumulants, rather than from a truncation at $O(\lambda^2)$. The same operator structure also arises in exact Gaussian TCL resummations [13].

Different environments enter the generator through the sum over bath indices. In structured spectral densities, where the index α labels distinct environmental modes coupled to the system, Markovian embedding approaches require introducing additional degrees of freedom for each mode [20]. The resulting enlarged Hilbert space therefore grows exponentially with the number of oscillators.

By contrast, the resummed TCL generator incorporates the influence of each mode through bath correlation functions and scales only linearly with the number of modes. The TCL approach therefore remains tractable even for highly structured environments containing a large number of spectral features.

As discussed above, this antisymmetry produces paired frequency components in the generator. The imaginary parts generated by the bath correlation function therefore enter with opposite signs for the two transitions. If the component associated with $\omega_{\text{in}}^{(j)}$ acquires a decay rate $\gamma_{\text{in}}^{(j)}(t) > 0$, the conjugate component necessarily acquires the rate $-\gamma_{\text{in}}^{(j)}(t)$. This also implies a proliferation of renormalized frequencies through the additional index j , although this additional structure is absent in the examples considered in the present paper.

Generator validity range. The generator $L(t)$ obtained from Ref. [6] establishes an internally consistent description up to a finite time scale t_L

$$t_L \approx \frac{s+1}{\nu_2}, \quad \nu_2 = \frac{1}{T_2},$$

where T_2 is the decoherence time. The estimate was obtained using a time-independent reference generator L_M introduced in Ref. [6]. This time corresponds to the minimum of the generator deviation $\|L(t) - L_M\|$: before t_L the norm decreases, while for $t > t_L$ it begins to increase as the growing modes of the generator become dominant.

The Davies generator L_0 (defined below) can also be used instead of L_M . The difference $\|L_M - L_0\|$ is time-independent and of order $O(\lambda^2)$, so by the triangle inequality the location of the minimum of $\|L(t) - L_0\|$ occurs at the same time scale. The definition of t_L is therefore not reference-dependent. Thus, thereafter we use L_0 as the standard reference generator.

For $t \ll t_L$ the time-local generator approaches the Davies weak-coupling generator L_0 defined below. As the difference $L(t) - L_0$ decreases the dynamics becomes

effectively Markovian on the van Hove time scale. The semigroup therefore acts as a transient fixed point of the time-local evolution.

For $t \gtrsim t_L$ the behavior reverses. The paired growth modes identified above prevail and the norm $\|L(t) - L_0\|$ begins to increase. The generator ceases to be a perturbation of L_0 and moves away from the Markovian regime. In the present work we effectively use $L(t)$ as input data on the interval $t \lesssim t_L$, where the cumulant resummation remains controlled but the growth modes are already visible. The dynamical map is then obtained by analytic continuation.

The reference generator L_0 is taken to be the Davies weak-coupling generator [21], i.e. the Markovian semigroup selected by the van Hove weak-coupling limit of the microscopic Hamiltonian:

$$L_0 = -i[H_S + H_{\text{LS}}, \cdot] + K_0, \quad (20)$$

where K_0 is the dissipator with matrix elements (see, e.g., Ref. [21, 22])

$$\begin{aligned} [K_0]_{nm,ij} = & \sum_{\alpha} 2 A_{ni}^{\alpha} A_{jm}^{\alpha} \delta_{\omega_{in}, \omega_{jm}} J_{\omega_{in}}^{\alpha} \\ & - \delta_{ni} \delta_{jm} \sum_{\alpha, k} \left(|A_{nk}^{\alpha}|^2 J_{\omega_{nk}}^{\alpha} + |A_{jk}^{\alpha}|^2 J_{\omega_{jk}}^{\alpha} \right). \end{aligned} \quad (21)$$

The Lamb-shift Hamiltonian H_{LS} has matrix elements

$$[H_{\text{LS}}]_{nm} = \delta_{nm} \sum_{\alpha, k} |A_{nk}^{\alpha}|^2 S_{\omega_{nk}}^{\alpha}. \quad (22)$$

The specialization of L_0 to the spin–boson model is given in Sec. VII A.

In the van Hove scaling $\tau = t\lambda^2$ the reduced dynamics converges to this semigroup,

$$\lim_{\lambda \rightarrow 0} \|\rho_{\text{ex}}(\tau/\lambda^2) - e^{L_0 \tau/\lambda^2} \rho(0)\| = 0, \quad (23)$$

so $e^{L_0 t}$ provides the leading reduced dynamics in this weak-coupling sense.

IV. FEYNMAN DISENTANGLEMENT THEOREM

To determine a dynamical map whose logarithmic derivative reproduces the resummed time-local generator, we parameterize the exact map relative to the contractive reference semigroup:

$$\rho_{\text{ex}}(t) = \Phi_{\text{ex}}(t)\rho(0) = (e^{L_0 t} + \mathbf{C}_{\text{ex}}(t))\rho(0). \quad (24)$$

Here $\mathbf{C}_{\text{ex}}(t)$ is an $O(\lambda^2)$ correction superoperator describing deviations from the reference evolution, with $\mathbf{C}_{\text{ex}}(0) = 0$ so that $\Phi(0) = \mathbb{I}$. [23]

The exact map satisfies the master equation

$$\dot{\Phi}_{\text{ex}}(t) = L_{\text{ex}}(t)\Phi_{\text{ex}}(t), \quad \Phi_{\text{ex}}(0) = 1. \quad (25)$$

Split the generator as

$$L_{\text{ex}}(t) = L_0 + \delta L(t). \quad (26)$$

The Feynman disentangling theorem then gives

$$\Phi_{\text{ex}}(t) = e^{L_0 t} \mathcal{T} \exp \left[\int_0^t d\tau e^{-L_0 \tau} \delta L(\tau) e^{L_0 \tau} \right]. \quad (27)$$

Equivalently,

$$\Phi_{\text{ex}}(t) = e^{L_0 t} \mathcal{T} \exp \left[\int_0^t d\tau e^{-L_0 \tau} (L_{\text{ex}}(\tau) - L_0) e^{L_0 \tau} \right]. \quad (28)$$

Since $\delta L(t) = O(\lambda^2)$, expansion to $O(\lambda^2)$ gives

$$\Phi_{\text{ex}}(t) = e^{L_0 t} \left[1 + \int_0^t d\tau e^{-L_0 \tau} \delta L(\tau) e^{L_0 \tau} \right] + O(\lambda^4). \quad (29)$$

Inserting the factor $e^{L_0 t}$ into the integral and comparing with Eq. (24), we identify the correction $\mathbf{C}_{\text{ex}}(t)$ to accuracy $O(\lambda^2)$ as

$$\mathbf{C}_{\text{ex}}(t) = \int_0^t d\tau e^{L_0(t-\tau)} (L_{\text{ex}}(\tau) - L_0) e^{L_0 \tau} + O(\lambda^4). \quad (30)$$

The singularity of the map can make the norm $\|L_{\text{ex}}(t)\|$ very large, but does not produce a corresponding growth of the dynamical map. Consequently the correction $\mathbf{C}_{\text{ex}}(t)$ also remains finite. The time integral in Eq. (30) suppresses the divergence of $L_{\text{ex}}(t)$ because the growth directions of the generator are weighted by the contractive Davies semigroup. It would therefore be incorrect to interpret the integral as a regularization of the generator. Rather, the forward semigroup action compensates the singular growth and reconstructs the second-order contribution to the dynamical map.

We now make the crucial step: the same contractive mechanism applies when $L_{\text{ex}}(t)$ is replaced by the partially resummed generator $L(t)$. What appears as an exponentially growing correction in the generator produces only a small contribution to the resulting map. This motivates defining an approximate map through

$$\mathbf{C}(t) = \int_0^t d\tau e^{L_0(t-\tau)} [L(\tau) - L_0] e^{L_0 \tau}. \quad (31)$$

The net map is then written as $e^{L_0 t} + \mathbf{C}(t)$, where the integral disentangles the map from the singular growth of the approximate generator. To avoid repeated terminology, we refer to this map interchangeably as the *reconstructed* or *disentangled* map.

In Eq. (31), the exponentially large deviations of the generator from L_0 are increasingly suppressed by the semigroup contraction as time progresses beyond t_L . By contrast, for times of order $t \lesssim t_L$, where $\|L(t) - L_0\|$ is still decreasing, the growing modes appear only as weak effects and are only partially suppressed by the contractive dynamics. As a result, the disentangled map effectively provides an analytic continuation of the resummed

TCL generator, anchored in the growing modes visible in the time window where the cumulant construction remains controlled. The corresponding reconstructed generator is then obtained by taking the logarithmic derivative.

Note that the result in Eq. (31) is nonperturbative because the truncation applies only to the disentanglement step, not to the generator $L(t)$, which is partially resummed and contains nested contributions from all orders of the interaction. Numerical results in this paper were obtained by solving the reconstruction equation

$$\dot{\mathbf{C}}(t) - L_0 \mathbf{C}(t) = [L(t) - L_0] e^{L_0 t}, \quad (32)$$

which is equivalent to Eq. (31) but provides improved numerical stability. The differential formulation also makes clear that the growing modes of $L(t)$ are preceded by the reference contraction.

Also note that separating the integrand into $L(\tau)$ and $-L_0$ parts gives

$$\mathbf{C}(t) = \int_0^t d\tau e^{L_0(t-\tau)} L(\tau) e^{L_0 \tau} - \int_0^t d\tau e^{L_0(t-\tau)} L_0 e^{L_0 \tau}, \quad (33)$$

since L_0 commutes with its exponential,

$$\int_0^t d\tau e^{L_0(t-\tau)} L_0 e^{L_0 \tau} = t e^{L_0 t} L_0. \quad (34)$$

Hence

$$\begin{aligned} \Phi(t) &= e^{L_0 t} - t e^{L_0 t} L_0 + \int_0^t d\tau e^{L_0(t-\tau)} L(\tau) e^{L_0 \tau} \\ &= e^{L_0 t} \left[I - t L_0 + \int_0^t d\tau e^{-L_0 \tau} L(\tau) e^{L_0 \tau} \right]. \end{aligned} \quad (35)$$

The last pair of equations show that the disentanglement procedure necessarily produces a linear-in-time contribution proportional to $t L_0$. A purely exponential decay therefore requires that the contribution generated by $L(\tau)$ provide an equal and opposite linear term. The existence of exponential relaxation thus imposes a constraint on the generator, as will be seen in the applications below.

V. RWA MODEL AND EXACT DYNAMICS

We consider the spin-boson model

$$H = H_S + H_B + H_I, \quad H_S = \frac{\Delta}{2} \sigma_z, \quad H_I = A \otimes F. \quad (36)$$

We specialize to unbiased transverse coupling,

$$A = \frac{1}{2} \sigma_x. \quad (37)$$

Throughout the main text we further restrict to zero temperature. Excitation processes are then absent, so

any loss of invertibility of the reduced dynamics cannot be attributed to thermal mixing and must instead originate from coherent system–bath interaction. In several expressions we write the matrix element A_{12}^2 explicitly as $1/4$; this factor should be understood as A_{12}^2 , A_{21}^2 , or $|A_{12}|^2$, depending on context, and thus the formalism extends trivially to an arbitrary transverse coupling direction.

In the rotating-wave approximation we retain only number-conserving terms,

$$H_I \approx \frac{1}{2}(\sigma_+ \otimes F_- + \sigma_- \otimes F_+), \quad (38)$$

$$F_+ = \sum_k g_k b_k^\dagger, \quad F_- = \sum_k g_k^* b_k, \quad (39)$$

so that the total excitation number $N = \sigma_+ \sigma_- + \sum_k b_k^\dagger b_k$ is conserved. At $T = 0$ the dynamics from a single-excitation preparation is therefore confined to the $N = 1$ sector.

For an initial superposition

$$|\Psi(0)\rangle = c_1|1\rangle + c_2|2\rangle, \quad |c_1|^2 + |c_2|^2 = 1, \quad (40)$$

the exact reduced state has the form [14]

$$\rho_{\text{exact}}(t) = \begin{bmatrix} |c_1 f(t)|^2 & c_1 c_2^* f(t) \\ c_1^* c_2 f^*(t) & 1 - |c_1 f(t)|^2 \end{bmatrix}, \quad (41)$$

corresponding to the quantum dynamical map

$$\Phi_f(t) = \begin{bmatrix} |f(t)|^2 & 0 & 0 & 0 \\ 1 - |f(t)|^2 & 1 & 0 & 0 \\ 0 & 0 & f^*(t) & 0 \\ 0 & 0 & 0 & f(t) \end{bmatrix}, \quad (42)$$

in the ordering $(\rho_{11}, \rho_{22}, \rho_{21}, \rho_{12})$. So all reduced dynamics is determined by the survival amplitude $f(t)$. The coherence sector contributes two singular values equal to $|f|$, while the population block yields one singular value of order $|f|^2$, and one of order unity. Hence, as $f(t) \rightarrow 0$ three singular values simultaneously vanish and the map approaches a rank-one projection.

The time-local generator is obtained by inserting Eq. (42) into Eq. (1):

$$L_f(t) = \begin{bmatrix} \dot{f} & \dot{f}^* & 0 & 0 & 0 \\ -\dot{f} & -\dot{f}^* & 0 & 0 & 0 \\ 0 & 0 & \dot{f}^* & 0 & 0 \\ 0 & 0 & 0 & 0 & \dot{f} \end{bmatrix}. \quad (43)$$

Consequently the time-local generator diverges at the zeros of the survival amplitude.

In the RWA model, the transverse Bloch component satisfies

$$\dot{x}(t) - iy(t) = 2\rho_{12}(t) = f(t)[x(0) - iy(0)].$$

Thus the evolution acts on the (x, y) plane as an isotropic contraction combined with a rotation.

In the interaction picture, $f_I(t) = e^{-i\Delta t} f(t)$ obeys the exact Volterra equation

$$\dot{f}_I(t) = -\frac{1}{4} \int_0^t d\tau C(t-\tau) e^{i\Delta(t-\tau)} f_I(\tau). \quad (44)$$

Equation (44) is identical to the survival–amplitude equation derived by Peres for quantum decay into a continuum spectrum [9]. In such systems the survival amplitude contains two distinct components: an exponential term associated with a pole of the resolvent, and a delayed correlation term arising from the continuum spectrum. As first shown by Khalin [8], the continuum part necessarily produces non-exponential long-time behavior. In the present model the same pole and branch-cut structure appears through the bath correlation function $C(t)$, which generates an algebraic tail that interferes with the exponential pole contribution.

The explicit solution in the Schrödinger picture is [14]

$$f(t) = \frac{1}{4\pi} \int_0^\infty d\omega \frac{e^{-i\omega t} J_\omega}{(\Delta - \omega + S_\omega/4)^2 + (J_\omega/4)^2}. \quad (45)$$

The integral representation confirms that the coherence amplitude remains finite and smooth for all times. Thus, a divergence of the logarithmic derivative $\dot{f}(t)/f(t)$ can occur only when the denominator becomes arbitrarily small. This realizes the mechanism anticipated in the Introduction: the reduced state remains regular while the dynamical map approaches loss of invertibility, and the singularity appears only in the logarithmic generator representation.

Equation (45) makes explicit that the survival amplitude is a Fourier transform of a bounded spectral density determined by the bath. Consequently the late-time behavior cannot remain purely exponential and must cross over to the algebraic decay.

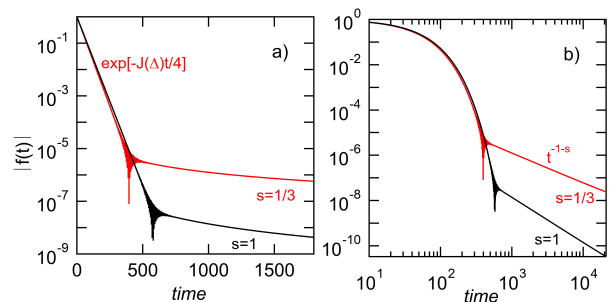


FIG. 2. Representative long-time dynamics of the coherence amplitude $|f(t)|$. (a,b) Log-linear and log-log plots showing the crossover from exponential (Markovian) to power-law (non-Markovian) decay. Near the phase lock-in time t_P , interference produces oscillations. Black: Ohmic bath ($s = 1$, $\lambda^2 = 0.025$); red: sub-Ohmic bath ($s = 1/3$, $\lambda^2 = 0.01$). In both cases $\omega_c = 4$, $\Delta = 1$.

Representative exact solutions for several spectral exponents are shown in Fig. 2. The coherence magnitude $|f(t)|$ crosses from an initial exponential decay to

a late-time algebraic tail at the time scale t_P , defined by Eq. (50). Near t_P , destructive interference between these two contributions produces deep minima in $|f(t)|$.

A. Pole-plus-tail interference

In the weak-coupling regime the integrand in Eq. (45) is sharply peaked near $\tilde{\Delta} = \Delta + S(\Delta)/4$. Expanding about this peak yields a Lorentzian lineshape and the Wigner-Weisskopf (Markovian) exponential contribution

$$f_M(t) = e^{-[i\tilde{\Delta} + J_{\Delta}/4]t}, \quad (46)$$

which accurately describes the coherence for $t \lesssim t_P$.

At late times the dominant frequencies scale as $\omega \sim 1/t$, and the lineshape in Eq. (45) is controlled by its low-frequency behavior. Rapidly oscillating contributions average out and only the low-frequency part of the spectrum survives. Approximating the denominator by its $\omega = 0$ value then gives the tail

$$f_C(t) \approx \frac{1}{4[\Delta + S_0/4]^2} C(t), \quad (47)$$

which captures the algebraic decay for $t \gtrsim t_P$. The exact coherence is therefore well approximated by the two-component form

$$f(t) \approx f_M(t) + f_C(t). \quad (48)$$

Destructive interference between f_M and f_C produces times at which $f(t)$ becomes anomalously small, approaching the kernel of the dynamical map.

The time t_P follows from the balance between the Markovian pole contribution and the long-time tail, $|f_M(t_P)| = |f_C(t_P)|$. From Eq. (46) one has $|f_M(t)| = e^{-t/T_2}$, while the bath correlator for a spectral density $J(\omega) \propto \omega^s e^{-\omega/\omega_c}$ yields the asymptotic tail $|f_C(t)| \propto (\omega_c t)^{-(s+1)}$. Equating the two gives

$$e^{-t_P/T_2} \sim (\omega_c t_P)^{-(s+1)}, \quad (49)$$

so that

$$\frac{t_P}{T_2} \sim (s+1) \ln(\omega_c t_P).$$

In the weak-coupling regime $\omega_c T_2 \gg 1$, replacing t_P inside the logarithm by T_2 up to subleading $\ln \ln$ corrections yields

$$\begin{aligned} t_P &\sim (s+1) T_2 \ln(\omega_c T_2) \\ &\sim (s+1) T_2 \ln \frac{1}{\lambda^2}. \end{aligned} \quad (50)$$

Near t_P , interference between f_M and f_C produces narrow modulation windows in $|f(t)|$, ranging from transient bursts to near-extinctions and accompanied by near- π phase slips at destructive interference [Fig. 3(a,b)].

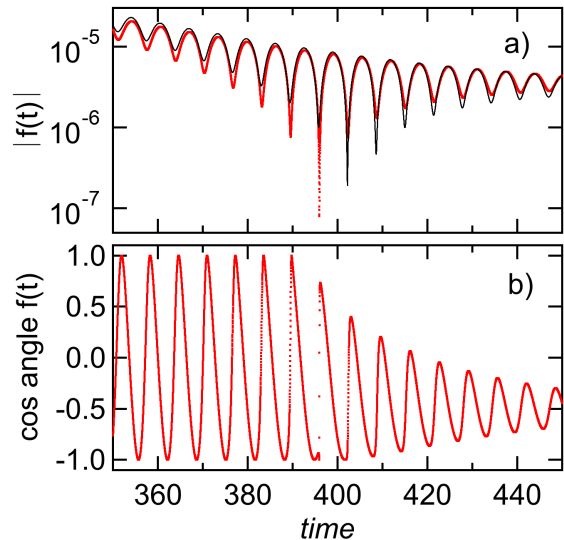


FIG. 3. Coherence magnitude (a) and phase (b) near t_P in the RWA model. Constructive interference produces bursts, while destructive interference leads to near-extinction. The phase undergoes a rapid rotation approaching a π slip, consistent with the map remaining invertible. Red dotted: exact solution; black solid: two-component model. Parameters: $s = 1/3$, $\lambda^2 = 0.01$, $\omega_c = 4$, $\Delta = 1$.

The dynamical map becomes strictly non-invertible only if $f(t) = 0$ at a finite time. For a continuum environment this requires exact destructive interference between the pole contribution and the bath-correlation tail. Such cancellation requires fine tuning of spectral phases and is therefore non-generic for continuum RWA-Hamiltonians. The interference produces very small but nonzero values of $f(t)$, so the map remains invertible at all finite times while approaching a non-invertible channel asymptotically.

VI. RWA CUMULANT EXPANSION

A. Reference and TCL Generators

We now apply the general cumulant analysis to the RWA Volterra equation (44) using the van Kampen ordered-cumulant expansion. As in the general case, for algebraically decaying bath correlation functions, cumulants beyond a critical order $n_{\max}(s)$ display late-time growth [6]. Resumming the leading growing cumulants reorganizes this algebraic growth into an exponential time dependence. This leading resummation is a special case of the complex renormalization introduced in Eq. (19) and defines the inflated TCL generator. Details are presented in Appendix B.

The time-dependent renormalized frequency is given

by

$$u(t) = \omega - \frac{i}{4}\Gamma_\omega(t), \quad (51)$$

while the survival amplitude in the interaction picture satisfies

$$\left. \frac{\dot{f}}{f} \right|_{\text{resum}} = -\frac{1}{4}\Gamma_{u(t)}(t) + O(\lambda^4). \quad (52)$$

The Schrödinger-picture partially resummed generator is then obtained from Eq. (43) by replacing \dot{f}/f with its resummed counterpart, yielding

$$L(t) = \begin{pmatrix} L_{\text{pop}}(t) & 0 \\ 0 & L_{\text{coh}}(t) \end{pmatrix}, \quad (53)$$

in the vectorization order $\rho_{11}, \rho_{22}, \rho_{21}, \rho_{12}$. Here

$$L_{\text{pop}}(t) = \frac{1}{2} \begin{pmatrix} -\text{Re}\Gamma_{u(t)}(t) & 0 \\ \text{Re}\Gamma_{u(t)}(t) & 0 \end{pmatrix}, \quad (54)$$

and

$$L_{\text{coh}}(t) = \begin{pmatrix} i\Delta - \frac{1}{4}\Gamma_{u(t)}^*(t) & 0 \\ 0 & -i\Delta - \frac{1}{4}\Gamma_{u(t)}(t) \end{pmatrix}. \quad (55)$$

The generator exhibits exponential growth at long times, since $\text{Im} u(t) < 0$ as $t \rightarrow \infty$.

Remark The full ordered-cumulant resummation contains nested renormalizations (Appendix B) that can shift the renormalized frequency onto a different analytic branch,

$$u = \omega - \frac{i}{4}\Gamma_{\omega - \frac{i}{4}\Gamma_{\omega - \frac{i}{4}\Gamma_{\omega - \dots}}}, \quad (56)$$

where we suppress the time dependence for clarity. Such branch shifts can qualitatively modify the long-time structure of the resummation, including its invertibility properties. In the present work we restrict the reconstruction to the analytic branch Eq. (51) that is continuously connected to the weak-coupling (Davies) limit. This choice preserves continuity with the microscopic weak-coupling theory and defines the branch used throughout. The role of the self-consistent renormalizations in Eq. (56) is left for future work.

B. Disentangled Map for the RWA

For the RWA Hamiltonian, the Davies generator decomposes into population and coherence sectors,

$$(L_0)_{\text{pop}} = \frac{1}{2} \begin{pmatrix} -J_\Delta & 0 \\ J_\Delta & 0 \end{pmatrix}, \quad (57)$$

and

$$(L_0)_{\text{coh}} = \begin{pmatrix} i\tilde{\Delta} - \frac{1}{4}J_\Delta & 0 \\ 0 & -i\tilde{\Delta} - \frac{1}{4}J_\Delta \end{pmatrix}. \quad (58)$$

Because $[L(t), L_0] = 0$, the reconstruction integral (31) simplifies to

$$\mathbf{C}(t) = e^{L_0 t} \int_0^t d\tau [L(\tau) - L_0]. \quad (59)$$

We define the complex Bohr frequency

$$z = \Delta - \frac{i}{4}\Gamma_\Delta. \quad (60)$$

Using the explicit matrices above, the reconstructed coherence amplitude $f(t) = \rho_{12}(t)/\rho_{12}(0)$ becomes

$$f(t) = \left(1 + \frac{\Gamma_\Delta}{4}t\right) e^{-izt} - \frac{1}{4}e^{-izt} \int_0^t d\tau \Gamma_{u(\tau)}(\tau). \quad (61)$$

The linear prefactor in front of the first exponential in Eq. (61) originates from the disentanglement identity Eq. (35). Its cancellation is clarified below.

1. Markovian Approximation for the Frequency

To obtain a closed analytic description of the dynamics, we consider the asymptotic regime $t \gg \tau_C$, where $\tau_C \equiv 1/\omega_c$ is the bath correlation time. The condition $t \gg \tau_C$ is typically associated with the onset of the Markovian limit [24].

In the regime $t \gg \tau_C$ we freeze the frequency renormalization in Eq. (51) at its asymptotic value and treat the pole as time independent,

$$u(t) \rightarrow z.$$

This is justified because the bath correlation function has already decayed on the scale τ_C , so the self-energy contribution entering $u(t)$ has reached its stationary limit.

In contrast, we retain the explicit time dependence of the memory kernel in Eqs. (54) and (55). The cumulant integral continues to grow and produces the large logarithmic derivative $\Gamma_z(t)$ even after the renormalized frequency has saturated. Consequently the late-time behavior is governed by a stationary pole but a time-dependent generator.

The resulting survival amplitude simplifies to

$$f(t) = \left(1 + \frac{1}{4}\Gamma_\Delta t\right) e^{-izt} - \frac{1}{4}\Sigma_z(t), \quad (62)$$

where

$$\Sigma_z(t) = \int_0^t d\tau \tau C(t-\tau) e^{-iz\tau} \quad (63)$$

is termed the diagonal kernel. It governs the late-time nonexponential decay of the survival amplitude.

The diagonal kernel admits the contour representation

$$\Sigma_z(t) = -\frac{1}{2\pi} \int_{-\infty+i\gamma}^{\infty+i\gamma} d\omega e^{-i\omega t} \frac{\Gamma_\omega}{(z-\omega)^2}, \quad (64)$$

where the contour offset $i\gamma$ lies above all singularities of the integrand. This form provides the starting point for the asymptotic analysis below.

2. Wigner–Weisskopf Regime

To leading order in λ^2 , the contour integral in Eq. (64) yields the survival amplitude

$$f(t) = e^{-izt} + \frac{1}{4\pi} \int_0^\infty d\omega \frac{e^{-i\omega t} \delta J_\omega}{(z - \omega)^2}, \quad (65)$$

where $\delta J_\omega = J_\omega - J_\Delta$.

The pole contribution together with the on-shell part of the branch cut on $\omega \in \mathbb{R}^+$ cancels the linear term $\Gamma_\Delta t/4$ generated by the disentanglement theorem, leaving the pure exponential decay of the van Hove limit. The remaining integral is the residual branch-cut correction.

3. Khalfin Regime

At long times the pole contribution has fully decayed, and the dynamics is governed entirely by the continuum component. The remaining amplitude is therefore determined by the highly oscillatory Fourier integral in (65), whose leading behavior is controlled by the analytic structure of the spectral density.

One obtains

$$f(t) \simeq \frac{C(t)}{4z^2}, \quad (66)$$

so that the coherence amplitude is directly proportional to the bath correlation function. This agrees, up to $O(\lambda^2)$ corrections in z , with the Khalfin long-time tail of the exact solution (47).

C. Exact Solution versus Continuation

Figure 4 verifies the analytic continuation procedure by solving the reconstruction equation (32) numerically, without invoking the asymptotic approximation $t \gg \tau_C$.

Panel (a) shows the early-time generator matrix element $L_{11,11}(t)$ obtained from the resummed TCL expansion and from the exact solution. The agreement demonstrates that the TCL generator captures the correct analytic structure at short times. This regime was termed “secular inflation” in Ref. [6], but that description is misleading in this time range, since the growth is physical and reproduced by the exact solution.

Panel (b) focuses on the time t_P where destructive interference strongly suppresses the survival amplitude $f(t)$ and the dynamical map becomes nearly singular. The generator reconstructed from the dynamical map matches the exact generator before, at, and after the spike, except at the very near-singular peaks. The agreement beyond the spike reflects that the map remains invertible, allowing the continuation procedure to recover the correct generator across the near-singular region.

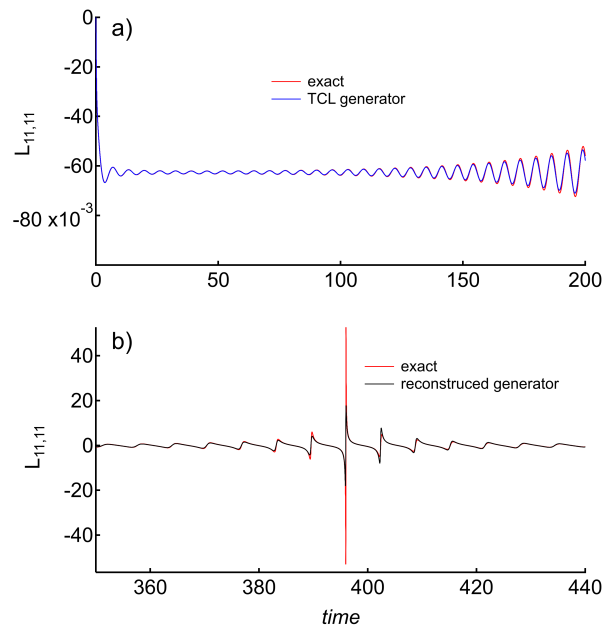


FIG. 4. **Numerical validation of the continuation procedure.** (a) Early-time generator element $L_{11,11}(t)$: resummed TCL (blue) agrees with the exact result (red). (b) Near t_P , destructive interference suppresses $f(t)$ and produces a sharp generator spike. The generator reconstructed from the disentangled map (black) reproduces the exact result (red) before, at, and after the spike. Parameters: $s = 1/3$, $\lambda^2 = 0.01$, $\omega_c = 4$, $\Delta = 1$, $T = 0$.

D. From the RWA to the Full Spin–Boson Model

With the RWA benchmark in hand, we now turn to the full spin–boson model. The RWA benchmark isolates the mechanism responsible for the generator spike: interference between the exponential pole and the algebraic correlation tail strongly suppresses the survival amplitude $f(t)$ and drives the dynamical map close to singularity. The map nevertheless remains invertible at all times, except for a measure-zero set of phase-matching conditions, admitting analytic continuation across the full time domain. In the full spin–boson model, however, counter-rotating terms induce nonsecular coherence transfer and introduce an anisotropy that becomes pronounced in the Khalfin regime. The resulting interference then converts the near-singular behavior of the survival amplitude into a true singularity.

VII. FULL SPIN-BOSON MODEL

We now consider a two-level system coupled to a bosonic environment through the full interaction term $A = \sigma_x/2$ in the Hamiltonian Eq. (36). The coupling operator A is the qubit observable to which the environment is sensitive. Information about the eigenstates

of A leaks into the bath, suppressing distinguishability between states that differ primarily along this direction. The central questions are: (i) what signatures of this anisotropy appear in the dynamics, and (ii) whether this suppression approaches rank deficiency only asymptotically, as in the RWA Hamiltonian, or reaches a noninvertible point at finite time.

A. Reference and TCL Generators in the SBM

The reference generator is given by Eqs. (57) and (58), with

$$\tilde{\Delta} = \Delta + \frac{1}{4}(S_{\Delta} - S_{-\Delta})$$

including the correct Lamb shift, in contrast to the naive rotating-wave approximation [25]. In the reference dynamics, the coherence evolves as a uniform contraction at rate $J_{\Delta}/4$ combined with a rotation at frequency $\tilde{\Delta}$. Because the contraction is isotropic, the singular values of the transverse propagator are equal and strictly positive for any finite time. Consequently the reference channel $\Phi_0(t)$ remains invertible for all $t < \infty$.

The TCL generator matrix elements are obtained by specializing the results of Appendix A to the unbiased spin-boson model at zero temperature. The population and coherence dynamics decouple, so the TCL generator reads

$$L(t) = \begin{pmatrix} L_{\text{pop}}(t) & 0 \\ 0 & L_{\text{coh}}(t) \end{pmatrix}. \quad (67)$$

The generator depends on a time-dependent renormalized transition frequency

$$\Delta'(t) = \Delta - \frac{i}{4}(\Gamma_{\Delta}(t) - \Gamma_{-\Delta}(t)). \quad (68)$$

For times $t \gg \tau_C$ the frequency approaches its Markovian limit

$$\Delta'(\infty) \equiv a = \Delta - \frac{i}{4}(\Gamma_{\Delta} + \Gamma_{-\Delta}^*) = \tilde{\Delta} - \frac{i}{4}J_{\Delta}. \quad (69)$$

In the following, analytical computations are performed within this Markov approximation for the frequency. Numerical computations, however, are carried out without this approximation by solving Eq. (32) directly.

For compactness we introduce the notation $\Gamma_{\pm}(t) \equiv \Gamma_{\pm\Delta'(t)}(t)$. The coherence block then takes the form

$$L_{\text{coh}}(t) = \begin{pmatrix} \ell_{21,21}(t) & \ell_{21,12}(t) \\ \ell_{12,21}(t) & \ell_{12,12}(t) \end{pmatrix}, \quad (70)$$

with matrix elements

$$\ell_{12,12}(t) = -i\Delta - \frac{1}{4}(\Gamma_{+}(t) + \Gamma_{-}(t)), \quad (71)$$

$$\ell_{21,12}(t) = \frac{1}{4}(\Gamma_{+}(t) + \Gamma_{-}^*(t)), \quad (72)$$

$$\ell_{21,21}(t) = \ell_{12,12}^*(t) \quad (73)$$

$$\ell_{12,21}(t) = \ell_{21,12}^*(t). \quad (74)$$

The diagonal elements contain the Bohr frequency Δ together with the dissipative combination $\Gamma_{+}(t) + \Gamma_{-}^*(t)$, which governs the decay of the coherence amplitudes. By contrast, the off-diagonal elements $\ell_{21,12}(t)$ and $\ell_{12,21}(t)$ generate nonsecular transfer between the two coherence components ρ_{12} and ρ_{21} . The dissipative parts of the secular and nonsecular sectors have equal magnitude and opposite sign, whereas only the secular rates contains the unitary splitting $-i\Delta$.

More generally, for a transverse coupling $A = \frac{1}{2}\vec{\sigma}\cdot\vec{a}$ in the plane orthogonal to the energy basis, the nonsecular coupling acquires a phase set by the pointer direction \vec{a} . The choice $A = \sigma_x/2$ used here yields a real coupling, whereas $A = \sigma_y/2$ would yield a purely imaginary one. By contrast, the diagonal decay rates are independent of the pointer direction. The anisotropy of the coherence dynamics is therefore carried by the phase of the nonsecular coherence channel.

The population block has an analogous structure,

$$L_{\text{pop}}(t) = \begin{pmatrix} \ell_{11,11}(t) & \ell_{11,22}(t) \\ \ell_{22,11}(t) & \ell_{22,22}(t) \end{pmatrix}, \quad (75)$$

with matrix elements

$$\ell_{11,11}(t) = -\frac{1}{2}\text{Re}\Gamma_{+}(t) \quad (76)$$

$$\ell_{11,22}(t) = \frac{1}{2}\text{Re}\Gamma_{-}(t) \quad (77)$$

$$\ell_{22,11}(t) = -\ell_{11,11}(t) \quad (78)$$

$$\ell_{22,22}(t) = -\ell_{11,22}(t). \quad (79)$$

B. Disentangled Map

Substituting the generator into the disentanglement formula Eq. (31) yields the matrix elements of the dynamical map. The intermediate algebra is given in the Appendix D.

In the coherence sector two distinct components appear,

$$\begin{aligned} \Phi_{12,12}(t) &= \left(1 + \frac{\Gamma_{\Delta} + \Gamma_{-\Delta}}{4}t\right)e^{-i\tilde{\Delta}t - \frac{J_{\Delta}}{4}t} \\ &\quad - \frac{1}{4}e^{-i\tilde{\Delta}t - \frac{J_{\Delta}}{4}t} \int_0^t d\tau [\Gamma_{\Delta'(\tau)}(\tau) + \Gamma_{-\Delta'(\tau)}^*(\tau)], \end{aligned} \quad (80)$$

and

$$\begin{aligned} \Phi_{21,12}(t) &= \frac{1}{4}e^{i\tilde{\Delta}t - \frac{J_{\Delta}}{4}t} \int_0^t d\tau e^{-2i\tilde{\Delta}\tau} \\ &\quad \times [\Gamma_{\Delta'(\tau)}(\tau) + \Gamma_{-\Delta'(\tau)}^*(\tau)]. \end{aligned} \quad (81)$$

The diagonal component contains the reference semi-group contribution together with a memory correction, whereas the off-diagonal component is generated entirely by the bath memory.

The other matrix elements are obtained by complex conjugation, $\Phi_{21,21} = \Phi_{12,12}^*$ and $\Phi_{12,21} = \Phi_{21,12}^*$. The linear prefactor in Eq. (80) is a non-Markovian term generated by the disentanglement theorem [see Eq. (35)]. It will be canceled by the integral contribution, restoring the van Hove limit.

The population dynamics can be reconstructed using the same disentanglement procedure as in the coherence sector. The calculation is algebraically more cumbersome because the population block couples the two diagonal components of the density matrix, so the main results are summarized in Subsubsection VII E, while the full derivation is deferred to Appendix D 3.

C. Diagonal Coherence Dynamics

The resulting integrals are evaluated in the Markov approximation for the frequency argument. The diagonal coherence element becomes

$$\Phi_{12,12}(t) = \left(1 + \frac{\Gamma_{\Delta} + \Gamma_{-\Delta}^*}{4}t\right)e^{-iat} - \frac{1}{4}\Sigma_a^{\text{sbm}}(t), \quad (82)$$

where

$$\Sigma_a^{\text{sbm}}(t) = \Sigma_a(t) + e^{-J_{\Delta}t/2} [\Sigma_{-a}(t)]^*, \quad (83)$$

with $\Sigma_a(t)$ defined in Eq. (63). The two terms represent the emission and absorption contributions, respectively.

As in the RWA, the diagonal kernel admits the contour representation

$$\Sigma_a^{\text{sbm}}(t) = -\frac{1}{2\pi} \int_{-\infty+i\gamma}^{\infty+i\gamma} d\omega e^{-i\omega t} \frac{\Gamma_{\omega} + [\Gamma_{-\omega^*+iJ_{\Delta}/2}]^*}{(\omega - a)^2}. \quad (84)$$

where the contour offset $i\gamma$ lies above all singularities of the integrand.

1. Diagonal Wigner-Weisskopf Regime in the SBM

As in the RWA, to leading order in λ^2 the contour integral yields

$$[\Phi(t)]_{12,12} = e^{-iat} + \frac{1}{4\pi} \int_0^{\infty} d\omega \left[\frac{e^{-i\omega t} \delta J_{\omega}}{(a - \omega)^2} + \frac{e^{i\omega t - J_{\Delta}t/2} J_{\omega}}{(a^* + \omega)^2} \right], \quad (85)$$

where $\delta J_{\omega} = J_{\omega} - J_{\Delta}$. The pole contribution together with the on-shell part of the branch cut on $\omega \in \mathbb{R}^+$ cancels the linear term $(\Gamma_{\Delta} + \Gamma_{-\Delta}^*)t/4$ generated by the disentanglement theorem, leaving the pure exponential decay of the van Hove limit. The remaining integral is the residual branch-cut correction.

2. Diagonal Khalfin Regime in the SBM

At long times $t \rightarrow \infty$, the dominant frequencies scale as $\omega \sim 1/t$, so the denominators may be expanded in ω . The leading term is then proportional to the bath correlation function, and the resulting Khalfin tail is

$$[\Phi(t)]_{12,12} = \frac{1}{4\Delta^2} [C(t) + e^{-J_{\Delta}t/2} C(t)^*]. \quad (86)$$

3. Pole-plus-tail interference

Combining the exponential and algebraic contributions yields the interpolation formula

$$\Phi_{12,12}(t) \approx e^{-iat} + \frac{1}{4\Delta^2} [C(t) + e^{-J_{\Delta}t/2} C(t)^*], \quad (87)$$

valid for $t \gg \tau_{\mathcal{C}}$.

The absorption contribution in Eq. (87) is subleading relative to the reference exponential e^{-iat} and therefore has little effect on the observable dynamics. Keeping only the leading part of each contribution, one may write

$$\Phi_{12,12}(t) \approx e^{-iat} + \frac{C(t)}{4\Delta^2}, \quad (88)$$

which provides a uniformly accurate interpolation for $t \gg \tau_{\mathcal{C}}$. Up to this point, the structure remains essentially the same as in the RWA model.

D. Off-diagonal coherence dynamics

The off-diagonal element differs qualitatively from the RWA case and therefore requires a separate analysis. It is central to the main results: anisotropy, the emergence of the pointer direction, projective behavior, and the loss of invertibility.

Since the off-diagonal map element is $O(\lambda^2)$, replacing $\tilde{\Delta}$ by Δ in nonoscillatory prefactors and denominators changes the result only at $O(\lambda^4)$. We make this replacement as convenient in the derivation, while retaining $\tilde{\Delta}$ in oscillatory phases and trigonometric functions, where the Lamb shift contributes to the long-time phase.

In the Markov approximation for the frequency, Eq. (81) can be rewritten as

$$\Phi_{21,12}(t) = \frac{1}{4} [Z_a(t) + e^{-J_{\Delta}t/2} [Z_{-a}(t)]^*], \quad (89)$$

where we introduced the offdiagonal kernel

$$Z_{x+iy}(t) = \int_0^t d\tau C(t-\tau) \frac{\sin(x\tau)}{x} e^{y\tau}. \quad (90)$$

Taking the Laplace transform and inverting along the Bromwich contour gives

$$\Phi_{21,12}(t) = -\frac{1}{8\pi} \int_{-\infty+i\gamma}^{\infty+i\gamma} d\omega e^{-i\omega t} \frac{\Gamma_{\omega} + [\Gamma_{-\omega^*+iJ_{\Delta}/2}]^*}{(\omega + iJ_{\Delta}/4)^2 - \tilde{\Delta}^2}. \quad (91)$$

The result separates naturally into pole and branch-cut contributions.

1. *Off-diagonal Wigner–Weisskopf regime in SBM*

Pole contribution. Evaluating the residues at $\omega_{\pm} = \pm\tilde{\Delta} - iJ_{\Delta}/4$ yields

$$\Phi_{21,12}^{\text{pole}}(t) = \frac{i}{8\tilde{\Delta}} e^{-J_{\Delta}t/4} \left[e^{-i\tilde{\Delta}t} \left(\Gamma_a + (\Gamma_{-a})^* \right) \right. \quad (92)$$

$$\left. - e^{+i\tilde{\Delta}t} \left(\Gamma_{-a^*} + (\Gamma_{a^*})^* \right) \right]. \quad (93)$$

In the weak-coupling limit $a \rightarrow \Delta - i0^+$, this reduces to

$$\Phi_{21,12}^{\text{pole}}(t) = -\frac{i}{4} e^{-J_{\Delta}t/4} \frac{\cos(\tilde{\Delta}t)}{\Delta} (\Gamma_{\Delta}^* + \Gamma_{-\Delta}), \quad (94)$$

which traces a one-dimensional trajectory in the complex plane.

Branch-cut contribution. The emission and absorption continua give

$$\Phi_{21,12}^{\text{cut}}(t) = -\frac{1}{4\pi} \int_0^{\infty} d\omega \frac{e^{-i\omega t} J_{\omega}}{(\omega + iJ_{\Delta}/4)^2 - \tilde{\Delta}^2} - \frac{e^{-J_{\Delta}t/2}}{4\pi} \int_0^{\infty} d\omega \frac{e^{i\omega t} J_{\omega}}{(\omega + iJ_{\Delta}/4)^2 - \tilde{\Delta}^2}. \quad (95)$$

Unlike the diagonal sector, the resolvent has only first-order poles. The on-shell and off-shell contributions can nevertheless be determined by contour deformation, as shown in Subsubsection D 2 d of Appendix D. One finds the on-shell contribution

$$\Phi_{21,12}^{\text{cut,em}}(t) = \frac{iJ_{\Delta}}{4\Delta} e^{-J_{\Delta}t/4} e^{-i\tilde{\Delta}t} \quad (96)$$

valid to $O(\lambda^2)$. The absorption integral has no pole in the upper half-plane and therefore produces only subleading off-resonant contributions.

Adding Eq. (96) to the pole term (94) yields the pole plus on-shell contribution

$$\Phi_{21,12}^{\text{pole+shell}}(t) = e^{-J_{\Delta}t/4} X(t), \quad (97)$$

where $X(t)$ is a real function

$$\begin{aligned} X(t) &= \frac{1}{4\Delta} \left[J_{\Delta} \sin(\tilde{\Delta}t) - (S_{\Delta} - S_{-\Delta}) \cos(\tilde{\Delta}t) \right] \\ &= \frac{1}{4} \frac{|\Gamma_{\Delta} + \Gamma_{-\Delta}^*|}{\Delta} \sin(\tilde{\Delta}t - \theta) \\ &= X_0 \sin(\tilde{\Delta}t - \theta). \end{aligned} \quad (98)$$

The phase is determined by the ratio of the Lamb shift to the spectral density,

$$\theta = \tan^{-1} \frac{S_{\Delta} - S_{-\Delta}}{J_{\Delta}}. \quad (99)$$

Thus the trajectory of $\Phi_{21,12}^{\text{pole+shell}}$ lies on the real axis in the complex plane. Because part of this anisotropy arises from the branch-cut contribution, the phase shift is not determined solely by the pole structure, but already carries a significant imprint of the continuum environment. As a result, a pole-only treatment such as Bloch–Redfield misses part of the anisotropy and predicts a different phase structure.

2. *Comparison with Bloch–Redfield dynamics*

Bloch–Redfield dynamics misses the branch-cut part of the anisotropy. In this case, the transfer amplitude $\Phi_{21,12}(t)$ becomes complex, with a phase that differs from that of the disentangled map.

The Bloch–Redfield map can be constructed explicitly by applying the disentanglement procedure of Sec. IV to the Bloch–Redfield generator. This generator is obtained from the partially resummed TCL generator by replacing the renormalized frequency (19) with the bare transition frequency in the dissipator (18). For example, Eq. (81) gives, in the Markovian approximation,

$$l_{21,12}(\tau) \rightarrow \frac{\Gamma_{\Delta} + \Gamma_{-\Delta}^*}{4}.$$

The corresponding nonsecular map element follows directly from Eq. (81) by replacing

$$\Gamma_{\Delta'(\tau)}(\tau) + \Gamma_{-\Delta'(\tau)}^*(\tau) \rightarrow \Gamma_{\Delta} + \Gamma_{-\Delta}^*$$

and performing the elementary integral:

$$\Phi_{21,12}^{\text{BR}}(t) = e^{-J_{\Delta}t/4} X^{\text{BR}}(t), \quad (100)$$

with

$$X^{\text{BR}}(t) = X_0 e^{i\theta} \sin(\tilde{\Delta}t). \quad (101)$$

The trajectory of $\Phi_{21,12}^{\text{BR}}(t)$ therefore lies along a line rotated by an angle θ with respect to the real axis, with no phase offset in the oscillation.

For consistency with numerical calculations that do not employ the Markovian approximation for the frequency, we also solve the Bloch–Redfield master equation with time-dependent coefficients in the numerical simulations [26].

The difference between Eqs. (98) and (101) is both qualitative and significant. In the disentangled map, the anisotropy is encoded as a phase shift of oscillations along the pointer axis. In Bloch–Redfield dynamics, by contrast, the same anisotropy appears instead as a rotation of the oscillation axis, with no phase shift.

Although the Bloch–Redfield generator is accurate to $O(\lambda^2)$, the coherence dynamics it generates need not be accurate to that order. Related inconsistencies of Bloch–Redfield dynamics have been discussed previously for population dynamics [5, 27–29]. Here the same issue arises in the coherence dynamics, not only quantitatively but also qualitatively, since Bloch–Redfield can

even predict the wrong anisotropy direction. This may appear to contradict the fact that the asymptotic coherence in Bloch–Redfield dynamics remains accurate to $O(\lambda^2)$ [5, 27–29]. However, the asymptotic amplitude can be correct even if the trajectory is not. More generally, this shows that correcting a master equation to reproduce the expected asymptotic state does not by itself guarantee dynamical accuracy [30].

The differences between the Bloch–Redfield, disentangled, and numerically exact TEMPO (time-evolving matrix product operator) dynamics [31] are illustrated in Fig. 5. To compare the oscillations, we project $\Phi_{21,12}^{\text{BR}}(t)$ onto its maximal quadrature by rotating out the trivial oscillatory phase,

$$\tilde{\Phi}_{21,12}^{\text{BR}}(t) = e^{-i\theta} \Phi_{21,12}^{\text{BR}}(t). \quad (102)$$

This aligns the signal with the direction of maximal oscillation amplitude, for which the orthogonal quadrature vanishes, as would be done experimentally when the pointer basis is not known a priori. The TEMPO results agree very closely with the disentangled map prediction, while the Bloch–Redfield results exhibit a systematic deviation due to the absence of the phase shift.

The amplitude of this anisotropy effect in $\Phi_{21,12}$ is $O(\lambda^2)$, but in this channel it contributes at leading order, since the reference contribution vanishes. It therefore appears already at early times, before the overall signal is strongly suppressed by exponential decay, and is in principle accessible by quantum process tomography.

Measuring the associated phase provides direct access to the bath correlation function and an early signature of the pointer direction. For example, in the scaling limit $\omega_c \rightarrow \infty$ for an Ohmic bath, $\theta \rightarrow -\pi/2$. In this regime, a detector coupled to a broadband electromagnetic environment, such as an Unruh–DeWitt detector, should exhibit the corresponding phase shift in its coherence dynamics.

3. Off-Diagonal Khalfin Tail in the SBM

The remaining off-shell continuum contribution to the disentangled map is evaluated in Subsection D 2 of Appendix D. Adding this contribution to the exponential part in Eq. (97) gives

$$\Phi_{21,12}(t) = e^{-J\Delta t/4} X(t) + \frac{C(t)}{4\Delta^2}. \quad (103)$$

This expression shares the same asymptotic tail as the diagonal coherence element in Eq. (88).

This reveals a sharp contrast between the Markovian regime and the late-time Khalfin-tail regime. In the Markovian regime, the nonsecular map element is suppressed by $O(\lambda^2)$ relative to the secular term. This suppression originates from the oscillatory structure of the interaction-picture generator: averaging over times of order T_2 reduces the nonsecular contribution and yields the asymmetry characteristic of the Davies semigroup.

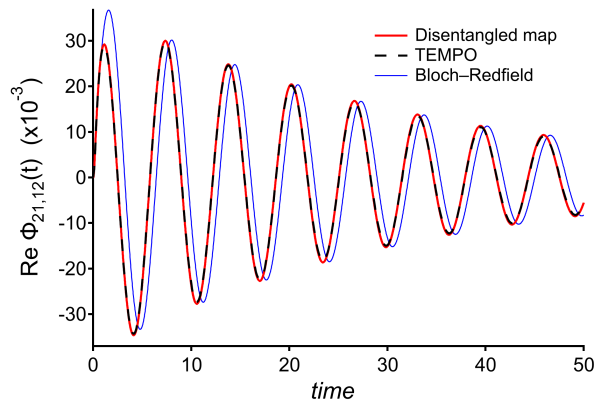


FIG. 5. Real part of the nonsecular transfer amplitude $\Phi_{21,12}(t)$. The disentangled map (red), obtained by numerically solving the reconstruction equation (32), is compared with TEMPO simulations (black dashed) and the Bloch–Redfield prediction (blue). The disentangled result agrees closely with TEMPO and shows that the anisotropy is encoded as a phase shift of oscillations along the pointer direction. Bloch–Redfield, which retains only the pole contribution, misses the branch-cut part of the anisotropy and instead predicts a rotated oscillation axis with no phase shift. The figure therefore provides an early-time, experimentally accessible signature of the continuum contribution that is absent in pole-only treatments. Parameters: $\Delta = 1$, $\omega_c = 4$, $s = 1$, $\lambda^2 = 0.025$, $\theta = -0.625$, $T = 0$.

In the Khalfin-tail regime, by contrast, this oscillatory averaging no longer controls the dynamics. The exponential contribution has already decayed, and the continuum tail dominates both secular and nonsecular elements. As a result, the secular and nonsecular map elements acquire the same asymptotic tail, and the Markovian asymmetry is lost. Understanding how Khalfin tails reorganize coherence hierarchies in multicoherence systems is an interesting direction for future work.

E. Population dynamics

The population dynamics can be reconstructed using the same disentanglement procedure as in the coherence sector. The derivation is more cumbersome and is given in Subsection D 3 of Appendix D.

The final result simplifies considerably. After cancellation of the disentanglement-induced linear term, the population map takes the affine form

$$\Phi_{\text{pop}}(t) = \begin{pmatrix} e^{-J\Delta t/2} & 0 \\ 1 - e^{-J\Delta t/2} & 1 \end{pmatrix} + B_\infty \begin{pmatrix} 1 & 1 \\ -1 & -1 \end{pmatrix}, \quad (104)$$

to leading order in λ^2 .

The stationary population is determined by

$$B_\infty = -\frac{1}{4} \partial_\omega S_\omega|_{-\Delta}, \quad (105)$$

which is an $O(\lambda^2)$ correction and coincides with the excited-state population of the mean-force Gibbs state.

The absence of a Khalfin tail in Eq. (104) is notable. Although the same algebra used to derive the coherence dynamics is applied here, no branch-cut contribution appears in the population sector. The populations therefore relax purely exponentially.

We note in passing that this contrasts with the RWA model, where the populations inherit the coherence tail, revealing a spurious feature of the approximation.

VIII. COMPLETE DYNAMICAL MAP FOR THE SBM

We now assemble the ingredients derived above. The reduced dynamics contains three distinct contributions: (i) Markovian relaxation and decoherence, described by the reference semigroup $e^{L_0 t}$; (ii) an exponentially damped nonsecular coherence term, given by Eq. (97); and (iii) the algebraic Khalfin tail, which follows from Eqs. (88) and (103),

$$[\Phi(t)]_{\text{coh,Khal}} = \frac{|C(t)|}{4\Delta^2} \begin{pmatrix} e^{-i\phi_c} & e^{i\phi_c} \\ e^{-i\phi_c} & e^{i\phi_c} \end{pmatrix}, \quad (106)$$

where $\phi_c = -\pi(s+1)/2$ is the phase of the bath correlation function.

Together they give the weak-coupling spin-boson dynamical map at zero temperature

$$\boxed{\Phi(t) = \Phi_{\text{GAD}}(t) + e^{-J\Delta t/4} X(t) \mathcal{T} + \frac{|C(t)|}{2\Delta^2} \mathcal{P}_{\text{coh}}.} \quad (107)$$

Equation (107) is valid to leading order in λ^2 . In particular, exponential decay rates are retained in resummed form, but their prefactors are evaluated at leading order, which depend on the matrix element, while all nonexponential contributions are included at $O(\lambda^2)$.

$\Phi_{\text{GAD}}(t)$ is the generalized amplitude-damping channel with relaxation parameter

$$\gamma(t) = 1 - e^{-J\Delta t/2}, \quad (108)$$

and excitation probability

$$p = B_\infty. \quad (109)$$

The operator $\mathcal{T}(\rho) = \rho^\top$ exchanges the coherence components $\rho_{12} \leftrightarrow \rho_{21}$ and generates a real, anisotropic nonsecular correction.

The Khalfin tail generates an asymptotic coherence block that is the coherence projection of a map consisting of a unitary rotation followed by projection onto the pointer axis

$$\mathcal{P}(\rho) = \sum_{\pm} P_{\pm} U_c^\dagger \rho U_c P_{\pm}, \quad (110)$$

where

$$P_{\pm} = \frac{1}{2}(I \pm \sigma_x), \quad U_c = e^{-i\phi_c \sigma_z/2}. \quad (111)$$

Note that Eq. (110) does not correspond to a rotation of the pointer axis. Rather, the state is first rotated and then projected onto the axis fixed by the interaction Hamiltonian.

Equation (107) is the central result of this work. It provides an explicit quantum dynamical map for the unbiased spin-boson model in the weak-coupling regime, separating the contributions of relaxation, nonsecular coherence mixing, and long-time projection driven by bath memory. It is completely positive and trace preserving up to corrections of order $O(\lambda^2)$.

A. Finite-time loss of invertibility

The three contributions in Eq. (107)—Markovian relaxation, nonsecular coherence mixing, and the Khalfin tail—play distinct roles whose combined action drives the smallest singular value of the dynamical map to zero at a finite time.

Let t_P denote the smallest time at which

$$|\Phi_{12,12}(t_P)| = |\Phi_{12,21}(t_P)|.$$

At this time the dynamical map loses invertibility.

This follows directly from the singular-value decomposition of the coherence block,

$$\begin{pmatrix} \Phi_{21,21}(t) & \Phi_{21,12}(t) \\ \Phi_{12,21}(t) & \Phi_{12,12}(t) \end{pmatrix},$$

whose singular values are

$$\sigma_{\pm}(t) = |\Phi_{12,12}(t)| \pm |\Phi_{12,21}(t)|. \quad (112)$$

Thus $\sigma_-(t_P) = 0$, signaling loss of invertibility.

The matrix elements follow directly from the map (107),

$$\Phi_{12,12}(t) = e^{-J\Delta t/4 - i\tilde{\Delta}t} + \frac{C(t)}{4\Delta^2}, \quad (113)$$

$$\Phi_{12,21}(t) = \frac{|\Gamma_{\Delta} + \Gamma_{-\Delta}^*|}{4\Delta} e^{-J\Delta t/4} \sin(\tilde{\Delta}t - \theta) + \frac{C(t)}{4\Delta^2}. \quad (114)$$

Both terms exhibit interference between an exponentially damped contribution and the bath correlation function. When their amplitudes become comparable, destructive interference suppresses the amplitude, though incomplete phase matching prevents exact cancellation in the individual terms, Eqs. (113) and (114).

The loss of invertibility ultimately arises because the secular and nonsecular components of the map share identical Khalfin tails but exhibit parametrically different Markovian components. The off-diagonal term is

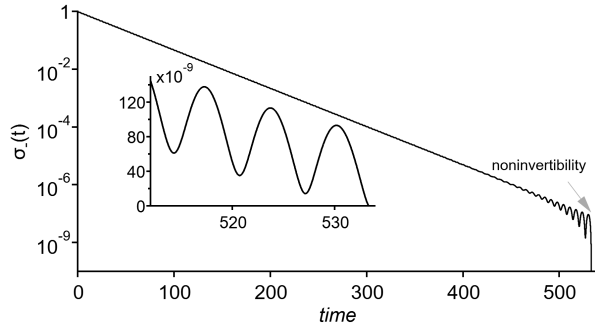


FIG. 6. Smallest singular value $\sigma_-(t)$ of the coherence component of the map. At early times, $\sigma_-(t)$ follows the exponential decay set by the Davies reference flow. At late times, interference between pole and branch-cut contributions produces oscillatory minima (inset) that drive $\sigma_-(t)$ to zero, marking noninvertibility. Same parameters as in Fig. 5.

$O(\lambda^2)$ and therefore enters the interference regime earlier. By the time the diagonal component reaches this regime, the off-diagonal contribution is already locked to the Khalfin tail. Destructive interference at the later time then suppresses the diagonal amplitude below the common Khalfin tail, forcing the two contributions to cross. At this crossing, a singular value vanishes and the dynamical map loses invertibility.

Thus, the crossing follows from three ingredients: Markovian decay, the Khalfin tail and its destructive interference with the Markovian decay, and the sharing of the same Khalfin tail by the secular and nonsecular components. The first two are independently established: exponential decay in the Davies limit and nonexponential late-time tails in the Khalfin–Peres theory of decay. The present derivation establishes the third. Once these three ingredients are recognized, the crossing follows directly and does not require following the full derivation in detail.

Beyond the crossing, the off-diagonal contribution exceeds the diagonal amplitude in magnitude, violating the CP condition. The Choi matrix then develops a negative eigenvalue, and any subsequent reopening of the singular value occurs outside the CPTP domain. As noted in the introduction, we therefore restrict the reconstructed dynamics to times up to the first zero.

Figure 6 shows the suppression of the singular value $\sigma_-(t)$ to zero. Prior to t_P , the environment suppresses the coherence amplitude, but the map remains invertible and the dynamics is reversible. At $t = t_P$, the crossing of amplitudes drives $\sigma_-(t)$ to zero, indicating irreversible loss of information about the initial state.

The finite-time collapse admits a natural interpretation in the language of measurement theory. While the interaction Hamiltonian defines the pointer axis in the sense of environment-induced superselection [32], the effective direction selected by the dynamics at finite times

is determined by the interference between the generalized amplitude-damping contribution and the Khalfin tail. Thus, the pointer axis directs the dynamics toward noninvertibility, but the actual collapse occurs along a dynamically selected direction set by the interplay of the different components of the map. In this sense, the collapse direction is not fixed by the pointer basis alone, but is determined by the interference of the dynamical contributions.

IX. DISCUSSION AND CONCLUSION

We have developed an analytic continuation procedure that reconstructs a nonperturbative dynamical map from divergent perturbative time-local generators. The method provides a controlled extrapolation beyond the regime of validity of perturbation theory, with very good agreement with the exactly solvable RWA model and with numerically exact TEMPO simulations at short times.

In the RWA, the dynamical map remains invertible at all times (except for a measure-zero set of phase-matching conditions), allowing analytic continuation across the full time domain. This establishes a benchmark for the method and clarifies that divergent generators arise from the time-local representation.

Applying the continuation procedure to the unbiased spin–boson model, we obtain a closed-form dynamical map at leading order and find that the smallest singular value vanishes at a time

$$t_P \sim (s + 1)T_2 \log(1/\lambda^2),$$

signaling a loss of invertibility. This effect is generated by the projective action of the continuum environment encoded in the Khalfin tail, which enforces a common long-time limit, while the secular and nonsecular components decay at the same rate in the early Markovian regime but with parametrically different amplitudes. As these components cross over to the common asymptotic tail at different times, destructive interference drives the singular value to zero before full convergence to that tail is reached.

The same continuum mechanism also produces an early-time anisotropy in the nonsecular coherence-transfer channel. This contribution is $O(\lambda^2)$, but leading in that channel since the reference term vanishes. The phase shift of this anisotropy is therefore, in principle, falsifiable by quantum process tomography. Its observation would provide clear evidence of the branch-cut influence of the continuum environment and an early signature of the mechanism that later drives the loss of invertibility.

More generally, the loss of invertibility reflects a transfer of quantum information from the subsystem into system–environment correlations, leading to a finite-time loss of distinguishability in the reduced dynamics. Extending the present framework to multicoherence systems may provide a useful setting for studying how this loss of

local distinguishability develops across larger coherence manifolds and how late-time continuum effects reorganize the information encoded in the reduced state.

This perspective also suggests possible applications to accelerated quantum systems. Acceleration-induced anisotropy may provide a framework in which information loss, quantum process tomography, and measurable signatures of acceleration-induced quantum noise can be analyzed within the present framework. Exploring these questions, including possible connections to Unruh-like phenomena, remains an interesting direction for future work.

A complementary arena where the present framework offers particular advantages is that of structured environments. The technique provides a scalable nonperturbative route to treating complex spectral densities, including coherence dynamics and energy transport in molecular and amorphous systems. This is especially relevant in settings where resonance-mediated transfer processes and dense vibronic structure both shape the dynamics [33, 34].

Several extensions of the present framework remain to be developed. A central next step is the inclusion of pure dephasing and finite-temperature environments, first at the qubit level. This is a fundamental extension rather than a routine one, since dephasing can qualitatively reorganize the reduced dynamics, including the crossover from Davies-type relaxation to Förster-like transport and the breakdown of simple thermalization behavior at intermediate dephasing. Additional directions include larger open quantum systems and multi-level, multicoherence settings. Together, these directions position the present work as a first step toward a broader nonperturbative description of open quantum system dynamics.

ACKNOWLEDGMENTS

The author thanks Jiahao Chen for valuable discussions and for extending the resummed TCL generator to the multi-bath regime, and Sirui Chen for helpful discussions. This work was supported by the School of Physics at the Georgia Institute of Technology through a seed grant. The author remains fully responsible for the content.

Appendix A: Partially Resummed TCL Generator for the Spin-Boson Model

This appendix provides an explicit representation of the partially resummed TCL generator to clarify the structure of Eqs. (18) and (19), whose physical content may be obscured by the density of indices in the main text. The expressions given here are intended both as a guide to interpretation and as a reference for practical implementation.

The formulation also serves as a starting point for future extensions of the present framework to finite temperature and biased spin-boson models, where spectral overlap play a significant role in the dynamics.

We write the time-local generator in the eigenbasis of the system Hamiltonian $H_S = \frac{\Delta}{2}\sigma_z$, where indices 1, 2 denote the eigenstates of σ_z . The system-bath coupling operator is written in this basis as $A_{nm} = \langle n|A|m\rangle$. We assume $A_{11} = -A_{22}$.

The bath enters through the correlation function

$$C(t) = \langle B(t)B(0)\rangle_\beta, \quad (\text{A1})$$

and its one-sided Fourier transform

$$\Gamma_\omega(t) = \int_0^t d\tau e^{i\omega\tau} C(\tau). \quad (\text{A2})$$

All correlation functions are evaluated at finite temperature. We also define the zero-frequency component

$$J_0(t) = \int_0^t d\tau C(\tau). \quad (\text{A3})$$

Excluding the spectral overlap, the interaction renormalizes the bare level splitting Δ into a time-dependent complex quantity

$$\Delta'(t) = \Delta - i|A_{12}|^2[\Gamma_\Delta(t) - \Gamma_{-\Delta}(t)]. \quad (\text{A4})$$

a. Role of the spectral-overlap shift. The partial resummation introduces a spectral-overlap shift of the renormalized splitting, such that the effective frequencies entering the bath response functions acquire imaginary contributions of the form $\Delta'(t) \pm 4iJ_0(t)A_{11}^2$. We therefore define

$$\Omega(t) = 4A_{11}^2J_0(t), \quad (\text{A5})$$

which approaches the asymptotic decay rate of the off-diagonal density-matrix elements (the transverse dephasing rate of the Davies generator) in the long-time limit.

The overlap shift enters the population sector with $+i\Omega(t)$, whereas the coherence block depends on $-i\Omega(t)$. This sign asymmetry has a direct dynamical consequence: the population dynamics is stabilized (broadening the effective transition frequencies appearing in the rates), while the coherence sector is destabilized, producing large or negative effective rates in the logarithmic time-local generator.

The generator preserves trace and Hermiticity of the density matrix. Consequently, its matrix elements satisfy

$$\sum_n L_{nn,ij}(t) = 0, \quad (\text{A6})$$

and

$$L_{nm,ij}(t) = L_{mn,ji}^*(t). \quad (\text{A7})$$

Therefore only an independent subset of components needs to be specified; all others follow from Eqs. (A6)–(A7).

b. *Population sector.*

$$L_{11,11}(t) = -2|A_{12}|^2 \operatorname{Re} \Gamma_{\Delta'(t)+i\Omega(t)}(t), \quad (\text{A8})$$

$$L_{11,22}(t) = 2|A_{12}|^2 \operatorname{Re} \Gamma_{-\Delta'(t)+i\Omega(t)}(t). \quad (\text{A9})$$

All remaining population elements follow from trace preservation, Eq. (A6).

c. *Population-coherence couplings.*

$$L_{21,11}(t) = 2A_{21}A_{11} [\Gamma_{\Delta'(t)+i\Omega(t)}(t) - iS_0(t)], \quad (\text{A10})$$

$$L_{21,22}(t) = 2A_{21}A_{11} [-\Gamma_{-\Delta'(t)+i\Omega(t)}^*(t) - iS_0(t)]. \quad (\text{A11})$$

All remaining couplings follow from the Hermiticity condition Eq. (A7).

d. *Coherence sector.*

$$L_{21,21}(t) = i\Delta - \Omega(t) - |A_{12}|^2 [\Gamma_{\Delta'(t)-i\Omega(t)}^*(t) + \Gamma_{-\Delta'(t)-i\Omega(t)}(t)], \quad (\text{A12})$$

$$L_{12,21}(t) = |A_{12}|^2 [\Gamma_{\Delta'(t)-i\Omega(t)}^*(t) + \Gamma_{-\Delta'(t)-i\Omega(t)}(t)]. \quad (\text{A13})$$

e. *Coherence-to-population transfer.* The coherence-to-population transfer term is

$$L_{11,21}(t) = 2A_{12}A_{11}J_0(t), \quad (\text{A14})$$

and trace preservation, Eq. (A6), implies $L_{22,21}(t) = -L_{11,21}(t)$. All other coherence elements are obtained from Eq. (A7).

These expressions completely determine the TCL generator for the qubit spin-boson model and reduce, in the zero-temperature limit, to the unbiased case discussed in the main text.

Appendix B: TCL Generator in the RWA

Roadmap. Starting from the Volterra iteration of the RWA survival amplitude, we (i) expand the solution into iterates f_n , (ii) construct the van Kampen cumulants K_{2n} via the recursion Eq. (B11), (iii) isolate the secular structure using the Δ -identity Eq. (B19), and (iv) show (to $O(\lambda^6)$) that the resulting cumulant series matches the nested-frequency form Eq. (B30).

1. Iterated solution and cumulant recursion

Integrating both sides of Eq. (44) from 0 to t and changing the order of integration yields a Volterra integral equation of the second kind,

$$f'(t) = 1 - \frac{1}{4} \int_0^t d\tau \Gamma_\omega(t-\tau) f'(\tau), \quad (\text{B1})$$

with the memory kernel $\Gamma_\omega(t)$ defined in Eq. (15), evaluated at $\omega = \Delta$. To reduce notational clutter, throughout

this appendix f is understood to be in the interaction picture (so we omit the prime). We use the shorthand for time ordered integrals as

$$\int \cdots \int_{\leftarrow}^t dt_{1\dots n} = \int_0^t dt_1 \int_0^{t_1} dt_2 \cdots \int_0^{t_{n-1}} dt_n.$$

Let us write down individual terms of the series obtained by iterating Eq. (B1). Defining $f(t) \equiv f_0 + f_1 + f_2 + f_3 + \dots$, we have

$$f_0 = 1, \quad (\text{B2})$$

$$f_1 = -\frac{1}{4} \int_0^t dt_1 \Gamma_\omega(t-t_1), \quad (\text{B3})$$

$$f_2 = \left(-\frac{1}{4}\right)^2 \iint_{\leftarrow}^t dt_{12} \Gamma_\omega(t-t_1) \Gamma_\omega(t_1-t_2), \quad (\text{B4})$$

$$f_3 = \left(-\frac{1}{4}\right)^3 \iiint_{\leftarrow}^t dt_{123} \Gamma_\omega(t-t_1) \Gamma_\omega(t_1-t_2) \Gamma_\omega(t_2-t_3). \quad (\text{B5})$$

For the derivatives we obtain

$$\dot{f}_0 = 0, \quad (\text{B6})$$

$$\dot{f}_1 = -\frac{1}{4} \Gamma_\omega(t), \quad (\text{B7})$$

$$\dot{f}_2 = \left(-\frac{1}{4}\right)^2 \int_0^t dt_1 \Gamma_\omega(t-t_1) \Gamma_\omega(t_1), \quad (\text{B8})$$

$$\dot{f}_3 = \left(-\frac{1}{4}\right)^3 \iint_{\leftarrow}^t dt_{12} \Gamma_\omega(t-t_1) \Gamma_\omega(t_1-t_2) \Gamma_\omega(t_2). \quad (\text{B9})$$

According to the van Kampen cumulant series, the coherence generator admits the expansion

$$\frac{\dot{f}}{f} = K_2 + K_4 + K_6 + \dots \quad (\text{B10})$$

Multiplying by f and collecting equal powers of λ^2 yields the recursive relation

$$K_{2n} = \dot{f}_n - \sum_{j=1}^{n-1} K_{2n-2j} f_j, \quad (\text{B11})$$

which is a special case of the general recursion for TCL cumulants [35]. The three lowest orders are

$$K_2 = \dot{f}_1, \quad (\text{B12})$$

$$K_4 = \dot{f}_2 - f_1 \dot{f}_1, \quad (\text{B13})$$

$$K_6 = \dot{f}_3 - f_1 \dot{f}_2 - f_2 \dot{f}_1 + f_1^2 \dot{f}_1. \quad (\text{B14})$$

Substituting the explicit iterates gives, for the RWA

model,

$$K_2 = -\frac{1}{4}\Gamma_\omega(t), \quad (\text{B15})$$

$$K_4 = \frac{1}{16} \int_0^t dt_1 [\Gamma_\omega(t-t_1) - \Gamma_\omega(t)]\Gamma_\omega(t_1), \quad (\text{B16})$$

$$\begin{aligned} K_6 = & -\frac{1}{4^3} \iint_{\leftarrow}^t dt_{12} \Gamma_\omega(t-t_1)\Gamma_\omega(t_1-t_2)\Gamma_\omega(t_2) \\ & + \frac{1}{4^3} \int_0^t dt_1 \Gamma_\omega(t_1) \int_0^t dt_2 \Gamma_\omega(t-t_2)\Gamma_\omega(t_2) \\ & + \frac{1}{4^3} \Gamma_\omega(t) \iint_{\leftarrow}^t dt_{12} \Gamma_\omega(t-t_1)\Gamma_\omega(t_1-t_2) \\ & - \frac{1}{4^3} \Gamma_\omega(t) \left[\int_0^t dt_1 \Gamma_\omega(t_1) \right]^2. \end{aligned} \quad (\text{B17})$$

2. Secular structure from the Δ identity

Define

$$D(t, t_1) = \Delta \Gamma_\omega(t, t_1) \equiv \Gamma_\omega(t) - \Gamma_\omega(t_1), \quad \Gamma \equiv \Gamma_\omega(t). \quad (\text{B18})$$

This satisfies the identity [6]

$$\int \cdots \int_{\leftarrow}^t dt_{1\dots n} D(t, t-t_n) = \frac{(-i)^n}{n!} \frac{\partial^n \Gamma_\omega(t)}{\partial \omega^n}. \quad (\text{B19})$$

Thus the Δ -structure suppresses polynomial secular terms ($\sim t^n$) in the time-ordered integrals; any residual secular growth is restricted to derivatives of $\Gamma_\omega(t)$, which become dominant for algebraically decaying $C(t)$.

Using Δ , the fourth-order cumulant becomes

$$\begin{aligned} K_4 = & \frac{1}{4^2} \int_0^t dt_1 D(t, t-t_1) [D(t, t_1) - \Gamma] \\ = & \frac{i}{4^2} \Gamma \frac{\partial \Gamma}{\partial \omega} + \frac{1}{4^2} \int_0^t dt_1 D(t, t-t_1) D(t, t_1) \quad (\text{B20}) \\ \equiv & \frac{i}{4^2} \Gamma \frac{\partial \Gamma}{\partial \omega} + \frac{1}{4^2} H_\omega(t), \end{aligned}$$

where we introduced

$$H_\omega(t) = \int_0^t dt_1 D(t, t-t_1) D(t, t_1). \quad (\text{B21})$$

Next, converting the double integrals in B17 into time-ordered form via

$$\begin{aligned} \int_0^t dt_1 X(t_1) \int_0^t dt_2 Y(t_2) = \\ \iint_{\leftarrow}^t dt_{12} [X(t_1)Y(t_2) + X(t_2)Y(t_1)], \end{aligned}$$

we obtain

$$\begin{aligned} K_6 = & -\frac{1}{4^3} \iint_{\leftarrow}^t dt_{12} \left\{ \right. \\ & [\Gamma - D(t, t-t_1)] [\Gamma - D(t, t_1-t_2)] [\Gamma - D(t, t_2)] \\ & - [\Gamma - D(t, t_1)] [\Gamma - D(t, t_2)] [2\Gamma - D(t, t-t_2) - D(t, t-t_1)] \\ & - \Gamma [\Gamma - D(t, t-t_1)] [\Gamma - D(t, t_1-t_2)] \\ & \left. + 2\Gamma [\Gamma - D(t, t_1)] [\Gamma - D(t, t_2)] \right\} \quad (\text{B22}) \\ = & K_6^D + K_6^{D^2} + K_6^{D^3}. \quad (\text{B23}) \end{aligned}$$

The cumulant structure removes the zeroth order in Δ , so the leading nonzero contributions are linear in Δ , with Δ^2 and higher powers subleading. Using Eq. (B19) and

$$\iint_{\leftarrow}^t dt_{12} D(t, t-t_1) = \iint_{\leftarrow}^t dt_{12} D(t, t_2),$$

the linear term yields

$$K_6^D = \frac{1}{4^3} \Gamma^2 \iint_{\leftarrow}^t dt_{12} D(t, t_2) = -\frac{1}{4^3} \frac{1}{2!} \Gamma^2 \frac{\partial^2 \Gamma}{\partial \omega^2}. \quad (\text{B24})$$

The quadratic contribution is

$$\begin{aligned} K_6^{D^2} = & -\frac{\Gamma}{4^3} \iint_{\leftarrow}^t dt_{12} \left\{ D(t, t_1-t_2) D(t, t_2) - D(t, t_1) D(t, t-t_2) \right. \\ & \left. - D(t, t_1) D(t, t-t_1) - D(t, t_2) D(t, t-t_2) \right\}. \end{aligned} \quad (\text{B25})$$

Using

$$\int_0^t d\tau \Gamma_\omega(\tau) = t\Gamma_\omega(t) + i \frac{\partial \Gamma_\omega(t)}{\partial \omega}, \quad (\text{B26})$$

and

$$\int_0^t dt_1 \Gamma_\omega(t_1) \Gamma_\omega(t-t_1) = t\Gamma_\omega^2(t) + 2i\Gamma_\omega(t) \frac{\partial \Gamma_\omega(t)}{\partial \omega} + H_\omega(t), \quad (\text{B27})$$

one finds that the secular ($\sim t$) parts cancel between the two lines of Eq. (B25), leaving only subleading contributions. The leading cubic term $K_6^{\Delta^3}$ remains finite and we keep it implicit.

Collecting terms gives

$$K_6 = \frac{\Gamma}{4^3} \left\{ \left[\frac{\partial \Gamma_\omega(t)}{\partial \omega} \right]^2 - i \frac{\partial H_\omega(t)}{\partial \omega} \right\} + K_6^{\Delta^3}. \quad (\text{B28})$$

3. Matching to nested frequency renormalization

Summing the cumulants to $O(\lambda^6)$ yields

$$\begin{aligned} K = & K_2 + K_4 + K_6 \\ = & -\frac{\Gamma}{4} + \frac{i}{4^2} \Gamma \frac{\partial \Gamma}{\partial \omega} + \frac{1}{4^2} H_\omega(t) - \frac{\Gamma^2}{2! 4^3} \frac{\partial^2 \Gamma}{\partial \omega^2} \\ & + \frac{\Gamma}{4^3} \left[\left(\frac{\partial \Gamma_\omega(t)}{\partial \omega} \right)^2 - i \frac{\partial H_\omega(t)}{\partial \omega} \right] + K_6^{\Delta^3}. \end{aligned} \quad (\text{B29})$$

One may verify that these terms coincide with the Taylor expansion of the nested-frequency form through $O(\lambda^6)$:

$$K = -\frac{1}{4}\Gamma_{\omega - \frac{i}{4}\Gamma_{\omega - \frac{i}{4}\Gamma_{\omega}}} + \frac{1}{4^2}H_{\omega - \frac{i}{4}\Gamma_{\omega}} + K_6^{D^3} + \dots \quad (\text{B30})$$

The first term exhibits frequency renormalizations nested to second order. Truncating Eq. (B30) at order $O(\lambda^2)$ gives

$$K(t) \approx -\frac{1}{4}\Gamma_{u(t)}(t), \quad u(t) = \omega - \frac{i}{4}\Gamma_{\omega}(t), \quad (\text{B31})$$

which yields the leading resummed quantities in Eqs. (51) and (52) of the main text.

If the frequency renormalization is iterated indefinitely, as implied by Eq. (B30), one obtains the self-consistent equation

$$u(t) = \omega - \frac{i}{4}\Gamma_{u(t)}(t), \quad (\text{B32})$$

which formally corresponds, in the limit $t \rightarrow \infty$, to the pole in the lower half-plane of the exact solution, Eq. (45), if such a solution existed. However, due to the multivalued nature of Γ_{ω} , no consistent solution exists in \mathbb{C} . Successive iterations lead to discontinuous changes in the frequency, between positive and negative imaginary parts.

This behavior is illustrated in Fig. 7, which shows the time evolution of the renormalized frequency (real part) for increasing nesting order. At low order, the dynamics remains smooth and weakly oscillatory. With each additional iteration, late-time oscillations become progressively more pronounced, reflecting the increasing sensitivity to the multivaluedness of Γ_{ω} . This sequence demonstrates the approach to the branch-cut, or Riemann-sheet, structure of the exact solution, which is recovered only in the infinite-order limit.

As a function of time, Eq. (B32) admits a unique solution up to a critical time $t_{\text{un}} < t_P$. Beyond this point, the solutions become multivalued and the dynamical map loses invertibility. To remain within the invertible regime, we therefore do not employ the fully nested solution and instead retain only a single iteration in the frequency renormalization.

Appendix C: Disentanglement in the RWA

These appendices present a unified derivation of the dynamical maps used in the main text. We begin with the RWA model, where the commuting structure allows the disentanglement formula to be evaluated in closed form and cleanly exposes the pole/branch-cut decomposition. The spin-boson appendices then build on this structure. The diagonal coherence channel follows the same logic with the addition of the absorption contribution, the off-diagonal channel develops the pole-plus-shell mechanism that determines the pointer direction,

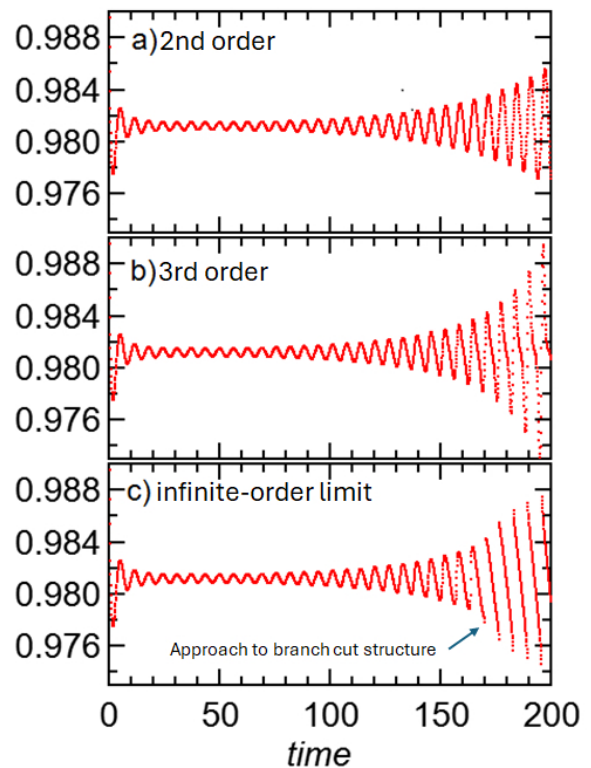


FIG. 7. Time evolution of the real part of the renormalized frequency for increasing nesting order of the frequency renormalization: (a) second order, (b) third order, and (c) higher-order nesting. As the nesting order increases, late-time oscillations become progressively enhanced, reflecting the approach to the branch-cut (Riemann-sheet) structure of the exact solution. The infinite-order limit corresponds to the nonperturbative continuum contribution. $s = 1/3$, $\lambda^2 = 0.01$, $\omega_c = 4$, $\Delta = 1$.

and the population sector reduces to an affine extension of the Davies semigroup without a Khalfin tail.

1. Reconstructed Dynamical Map in the RWA Model

We derive the reduced dynamical map for the rotating-wave (RWA) model directly from the disentanglement integral (C4).

The reduced state obeys the time-local master equation

$$\frac{d}{dt}\rho(t) = L(t)\rho(t). \quad (\text{C1})$$

Let

$$L_0 = \lim_{t \rightarrow \infty} L(t) \quad (\text{C2})$$

denote the asymptotic (Davies) generator. The exact dynamical map may be written as

$$\rho(t) = \Phi(t)\rho(0), \quad \Phi(t) = e^{L_0 t} + \mathbf{C}(t), \quad (\text{C3})$$

with

$$\mathbf{C}(t) = \int_0^t d\tau e^{L_0(t-\tau)} [L(\tau) - L_0] e^{L_0\tau}. \quad (\text{C4})$$

2. RWA simplification

For the RWA Hamiltonian, the TCL generator and the Davies generator are diagonal in the Bohr operator basis and therefore commute,

$$[L(t), L_0] = 0. \quad (\text{C5})$$

Hence the exponentials in Eq. (C4) commute with $L(\tau) - L_0$, and the reconstruction simplifies to

$$\mathbf{C}(t) = e^{L_0 t} \int_0^t d\tau [L(\tau) - L_0]. \quad (\text{C6})$$

3. Coherence dynamics in the RWA

Projecting onto the coherence operator $|1\rangle\langle 2|$ gives

$$f(t) = \frac{\rho_{12}(t)}{\rho_{12}(0)} = [\Phi(t)]_{12,12}. \quad (\text{C7})$$

Let the eigenvalue of L_0 in this sector be

$$[L_0]_{12,12} = -iz, \quad z = \Delta - \frac{i}{4}\Gamma_\Delta. \quad (\text{C8})$$

Using Eq. (C6),

$$[\mathbf{C}(t)]_{12,12} = \frac{e^{-izt}}{4} \left[\Gamma_\Delta t - \int_0^t d\tau \Gamma_{u(\tau)}(\tau) \right]. \quad (\text{C9})$$

For times $t \gg \tau_C$, the Markov approximation for the frequency applies,

$$u(\tau) \simeq z.$$

Using the bath correlation kernel

$$\Gamma_z(t) = \int_0^t d\tau' C(\tau') e^{iz\tau'}, \quad (\text{C10})$$

we obtain

$$\int_0^t d\tau \int_0^\tau d\tau' C(\tau') e^{iz\tau'} = \int_0^t d\tau' C(\tau') e^{iz\tau'} (t - \tau'). \quad (\text{C11})$$

Define the diagonal kernel

$$\Sigma_z(t) = \int_0^t d\tau \tau C(t - \tau) e^{-iz\tau}. \quad (\text{C12})$$

Then

$$[\mathbf{C}(t)]_{12,12} = \frac{\Gamma_\Delta t}{4} e^{-izt} - \frac{1}{4} \Sigma_z(t), \quad (\text{C13})$$

from which Eq. (62) in the main text follows.

4. Spectral representation

The Laplace transform of Eq. (C12) is

$$\tilde{\Sigma}_z(s) = \frac{\tilde{C}(s)}{(s + iz)^2}, \quad (\text{C14})$$

where

$$\tilde{C}(s) = \int_0^\infty dt e^{-st} C(t) \quad (\text{C15})$$

is the ordinary Laplace transform of the bath correlation function.

Using the standard spectral representation

$$C(t) = \frac{1}{\pi} \int_0^\infty d\omega J_\omega e^{-i\omega t}, \quad (\text{C16})$$

one also defines the half-sided Fourier-Laplace transform

$$\Gamma_\omega = J_\omega + iS_\omega = \int_0^\infty dt C(t) e^{i\omega t}. \quad (\text{C17})$$

The quantity Γ_ω is simply the Laplace transform $\tilde{C}(s)$ evaluated at $s = -i\omega$ by analytic continuation

We evaluate the inverse transform using the Bromwich contour,

$$\begin{aligned} \Sigma_z(t) &= \frac{1}{2\pi i} \int_{-i\infty+i\gamma}^{i\infty+i\gamma} ds e^{st} \tilde{\Sigma}_z(s) \\ &= \frac{1}{2\pi} \int_{-\infty+i\gamma}^{\infty+i\gamma} d\omega e^{-i\omega t} \tilde{\Sigma}_z(\omega), \end{aligned} \quad (\text{C18})$$

where the contour offset $i\gamma$ lies above all singularities of the integrand. Thus

$$\Sigma_z(t) = -\frac{1}{2\pi} \int_{-\infty+i\gamma}^{\infty+i\gamma} d\omega e^{-i\omega t} \frac{\Gamma_\omega}{(z - \omega)^2}. \quad (\text{C19})$$

which is Eq. (64) of the main text.

For $t > 0$, the factor $e^{-i\omega t}$ suppresses the contribution from the large semicircle in the lower half-plane, so the contour may be deformed downward. The analytic continuation of Γ_ω to the lower half-plane contains a branch cut on the positive real axis, while $(z - \omega)^{-2}$ produces a second-order pole at $\omega = z$. Therefore

$$\Sigma_z(t) = \Sigma_z^{\text{pole}}(t) + \Sigma_z^{\text{bc}}(t), \quad (\text{C20})$$

with

$$\Sigma_z^{\text{pole}}(t) = i \text{Res}_{\omega=z} \left[e^{-i\omega t} \frac{\Gamma_\omega}{(z - \omega)^2} \right], \quad (\text{C21})$$

and

$$\Sigma_z^{\text{bc}}(t) = -\frac{1}{2\pi} \int_0^\infty d\omega e^{-i\omega t} \frac{\Gamma_\omega^+ - \Gamma_\omega^-}{(z - \omega)^2}. \quad (\text{C22})$$

Here

$$\Gamma_\omega^\pm \equiv \lim_{\epsilon \downarrow 0} \Gamma_{\omega \pm i\epsilon} \quad (\text{C23})$$

denote the boundary values on the two sides of the branch cut.

5. Pole contribution from the Bromwich contour

We now evaluate the residue term in Eq. (C21). Since the only isolated singularity enclosed by the deformed contour is the second-order pole at $\omega = z$,

$$\begin{aligned} \text{Res}_{\omega=z} \left[\frac{\Gamma_\omega e^{-i\omega t}}{(z-\omega)^2} \right] &= \frac{d}{d\omega} \left(\Gamma_\omega e^{-i\omega t} \right) \Big|_{\omega=z} \\ &= (\partial_\omega \Gamma_\omega - it \Gamma_\omega)_{\omega=z} e^{-izt}. \end{aligned} \quad (\text{C24})$$

Therefore

$$\Sigma_z^{\text{pole}}(t) = e^{-izt} \left[t \Gamma_z + i \partial_\omega \Gamma_\omega \Big|_z \right]. \quad (\text{C25})$$

Substituting this into Eq. (C20) and then into Eqs. (C13) and (C3) gives

$$\begin{aligned} [\Phi(t)]_{12,12} &= \left(1 + \frac{\Gamma_\Delta t}{4} \right) e^{-izt} - \frac{1}{4} e^{-izt} \left[t \Gamma_z + i \partial_\omega \Gamma_\omega \Big|_z \right] \\ &\quad - \frac{1}{4} \Sigma_z^{\text{bc}}(t) \\ &= \left(1 + \frac{\Gamma_\Delta - \Gamma_z}{4} t - \frac{i}{4} \partial_\omega \Gamma_\omega \Big|_z \right) e^{-izt} - \frac{1}{4} \Sigma_z^{\text{bc}}(t). \end{aligned} \quad (\text{C26})$$

6. Branch discontinuity and the $2J_\Delta$ identity

The Sokhotski–Plemelj identity for the half-sided transform implies

$$\Gamma_\omega^+ - \Gamma_\omega^- = 2J_\omega. \quad (\text{C27})$$

The Davies rate is the upper boundary value,

$$\Gamma_\Delta = \Gamma_\Delta^+,$$

whereas $z = \Delta - i\Gamma_\Delta/4$ lies in the lower half-plane, so

$$\Gamma_z = \Gamma_\Delta^- + (z - \Delta) \partial_\omega \Gamma_\omega^- \Big|_\Delta + O(\lambda^6),$$

since $z - \Delta = O(\lambda^2)$ and $\partial_\omega \Gamma_\omega = O(\lambda^2)$. Thus

$$\Gamma_\Delta - \Gamma_z = 2J_\Delta - (z - \Delta) \partial_\omega \Gamma_\omega^- \Big|_\Delta + O(\lambda^4). \quad (\text{C28})$$

At the time scale $t \sim T_1 = 2/J_\Delta$, substituting into Eq. (C26) yields the leading contribution

$$[\Phi(t)]_{12,12} \approx \left(1 + \frac{J_\Delta t}{2} \right) e^{-izt} - \frac{1}{4} \Sigma_z^{\text{bc}}(t). \quad (\text{C29})$$

The pole contribution alone therefore does not restore exponential decay.

7. Evaluation of the branch-cut integral

Split

$$J_\omega = J_\Delta + \delta J_\omega.$$

The constant part gives the on-shell contribution,

$$\Sigma_{\text{bc,shell}}(t) = -\frac{J_\Delta}{\pi} \int_{-\infty}^{\infty} d\omega \frac{e^{-i\omega t}}{(z-\omega)^2}. \quad (\text{C30})$$

Closing the contour in the lower half-plane, the second-order pole at z yields

$$\int_{-\infty}^{\infty} d\omega \frac{e^{-i\omega t}}{(z-\omega)^2} = -2\pi t e^{-izt}. \quad (\text{C31})$$

Therefore

$$\Sigma_{\text{bc,shell}}(t) = 2J_\Delta t e^{-izt}. \quad (\text{C32})$$

8. Wigner–Weisskopf Regime in the RWA

Using Eqs. (C22), (C29), and (C32), we obtain

$$\begin{aligned} [\Phi(t)]_{12,12} &= \left(1 + \frac{J_\Delta t}{2} \right) e^{-izt} - \frac{J_\Delta t}{2} e^{-izt} \\ &\quad + \frac{1}{4\pi} \int_0^\infty d\omega \frac{e^{-i\omega t} \delta J_\omega}{(z-\omega)^2}. \end{aligned} \quad (\text{C33})$$

The two linear contributions cancel, leaving the exponential as the leading behavior:

$$[\Phi(t)]_{12,12} = e^{-izt} + \frac{1}{4\pi} \int_0^\infty d\omega \frac{e^{-i\omega t} \delta J_\omega}{(z-\omega)^2}. \quad (\text{C34})$$

This is Eq. (65) of the main text.

9. Khalfin regime in the RWA

At late times the exponential term in Eq. (C34) may be neglected, so

$$f(t) \simeq \frac{1}{4\pi} \int_0^\infty d\omega \frac{e^{-i\omega t} J_\omega}{(z-\omega)^2}. \quad (\text{C35})$$

On the chosen analytic branch, z lies in the lower half-plane, so the denominator never vanishes for real $\omega \geq 0$. For standard spectral densities the integrand is absolutely integrable, and the Riemann–Lebesgue lemma implies $f(t) \rightarrow 0$ as $t \rightarrow \infty$.

At large times the integral is dominated by low frequencies. Expanding the denominator around $\omega = 0$ gives

$$\frac{1}{(z-\omega)^2} = \frac{1}{z^2} + O(\omega), \quad (\text{C36})$$

so that

$$f(t) \simeq \frac{1}{4z^2} \frac{1}{\pi} \int_0^\infty d\omega e^{-i\omega t} J(\omega) = \frac{C(t)}{4z^2}. \quad (\text{C37})$$

This is Eq. (66) of the main text.

Appendix D: Disentanglement in the Spin–Boson Model

Before proceeding, we note that all analytic expressions in this and the previous appendix were verified against numerical solutions of the reconstruction equation (32), providing an independent check of the Laplace transforms and contour manipulations used in this paper.

1. Diagonal Coherence Dynamics

This channel differs from the RWA derivation only by the additional absorption contribution, so the pole/branch–cut analysis can be reused almost verbatim.

The disentanglement of the diagonal coherence element in the spin–boson model proceeds analogously to the RWA Hamiltonian. The explicit matrix element reads

$$\begin{aligned} \Phi_{12,12}(t) &= e^{(L_0)_{12,12}t} + \int_0^t d\tau e^{(L_0)_{12,12}(t-\tau)} \\ &\quad \times [l_{12,12}(\tau) - (L_0)_{12,12}] e^{(L_0)_{12,12}\tau} \\ &= \left[1 + \frac{1}{4}(\Gamma_\Delta + \Gamma_{-\Delta}^*)t \right] e^{-iat} \\ &\quad - \frac{1}{4}e^{-iat} \int_0^t d\tau \left[\Gamma_{\Delta'(\tau)}(\tau) + [\Gamma_{-\Delta'(\tau)}(\tau)]^* \right], \end{aligned} \quad (\text{D1})$$

which yields Eq. (80) of the main text. The two terms in the integrand represent the emission and absorption contributions, respectively.

For $t \gg \tau_C$ we employ the Markov approximation for the frequency,

$$\Delta'(t) \simeq a = \tilde{\Delta} - iJ_\Delta/4, \quad \Gamma_\pm(\tau) \equiv \Gamma_{\pm a}(\tau),$$

which gives Eq. (82) of the main text,

$$\Phi_{12,12}(t) = \left(1 + \frac{\Gamma_\Delta + \Gamma_{-\Delta}^*}{4}t \right) e^{-iat} - \frac{1}{4}\Sigma_a^{\text{sbm}}(t), \quad (\text{D2})$$

where

$$\Sigma_a^{\text{sbm}}(t) = e^{-iat} \int_0^t d\tau \left[\Gamma_a(\tau) + [\Gamma_{-a}(\tau)]^* \right]. \quad (\text{D3})$$

Proceeding as in Eq. (C11), the time integration yields Eq. (83) of the main text,

$$\Sigma_a^{\text{sbm}}(t) = \Sigma_a(t) + e^{-J_\Delta t/2} [\Sigma_{-a}(t)]^*, \quad (\text{D4})$$

with Laplace transform

$$\tilde{\Sigma}_a^{\text{sbm}}(s) = \frac{\tilde{C}(s) + [\tilde{C}(s^* + J_\Delta/2)]^*}{(s + ia)^2}. \quad (\text{D5})$$

Equivalently, in Fourier–Laplace form with $s = -i\omega$ and $\tilde{C}(s) = \Gamma_\omega$,

$$\tilde{\Sigma}_a^{\text{sbm}}(\omega) = -\frac{\Gamma_\omega + [\Gamma_{-\omega^* + iJ_\Delta/2}]^*}{(\omega - a)^2}. \quad (\text{D6})$$

The two terms in the numerator represent emission and absorption, respectively.

The inverse Laplace transform is evaluated using a Bromwich contour,

$$\Sigma_a^{\text{sbm}}(t) = \frac{1}{2\pi} \int_{-\infty+i\gamma}^{\infty+i\gamma} d\omega \tilde{\Sigma}_a^{\text{sbm}}(\omega) e^{-i\omega t}. \quad (\text{D7})$$

Inserting Eq. (D6) into Eq. (D7) yields Eq. (84) of the main text.

The emission contribution is identical to the RWA case, so the pole–plus–branch–cut analysis of the previous appendix applies after the substitution $z \rightarrow a$. In particular, the linear term $\Gamma_\Delta t/4$ in Eq. (D1) is canceled by the emission pole together with its on–shell branch–cut contribution.

Similarly, the pole in the absorption term cancels the non–Markovian term $(\Gamma_{-\Delta}^* t/4)e^{-iat}$, since $J_{-\Delta} = 0$. This restores the purely exponential Markovian limit.

The remaining branch–cut integral at $\omega^* = iJ_\Delta/2$ arising from the absorption contribution is evaluated by the substitution $\omega = -\omega' + iJ_\Delta/2$, which leads to the final integral in Eq. (85) of the main text.

2. Off-diagonal coherence dynamics.

The evaluation proceeds in three steps. First, the coherence kernel is written in terms of the bath correlation function, leading to the representation Eq. (D14). Second, the Laplace transform allows the dynamics to be expressed as a Bromwich contour integral, whose analytic structure separates naturally into pole and continuum contributions. Finally, we evaluate these contributions: the poles and the on–shell branch–cut component produce the exponential decay and determine the pointer direction, while the off–shell branch–cut component generates the non–Markovian continuum correction and the Khalfin tail.

a. Time-domain representation

The off-diagonal element $\Phi_{21,12}(t) = C_{21,12}(t)$ reads

$$\begin{aligned} \Phi_{21,12}(t) &= \int_0^t d\tau e^{(L_0)_{21,21}(t-\tau)} l_{21,12}(\tau) e^{(L_0)_{12,12}\tau} \\ &= e^{ia^*t} \int_0^t d\tau e^{-2i\tilde{\Delta}\tau} l_{21,12}(\tau). \end{aligned} \quad (\text{D8})$$

where $l_{21,12}(t)$ is given by Eq. (72). This yields

$$\begin{aligned} \Phi_{21,12} &= \Phi_{21,12}^{\text{emi}} + \Phi_{21,12}^{\text{abs}} \\ &= \frac{1}{4}e^{ia^*t} \int_0^t d\tau e^{-2i\tilde{\Delta}\tau} \\ &\quad \times \left[\Gamma_{\Delta'(\tau)}(\tau) + (\Gamma_{-\Delta'(\tau)}(\tau))^* \right]. \end{aligned} \quad (\text{D9})$$

Employing the Markovian approximation for the frequency $\Delta'(t) \simeq a$ gives an emission integral

$$\begin{aligned} I(t) &= \int_0^t d\tau e^{-2i\tilde{\Delta}\tau} \Gamma_{\Delta'}(\tau) \\ &= \int_0^t d\tau e^{-2i\tilde{\Delta}\tau} \int_0^\tau dx C(x) e^{iax} \end{aligned} \quad (\text{D10})$$

Interchanging the order of integration and performing the τ -integration yields

$$I(t) = \int_0^t dx C(t-x) e^{-i\tilde{\Delta}t + \frac{J\tilde{\Delta}}{4}(t-x)} \frac{\sin(\tilde{\Delta}x)}{\tilde{\Delta}}. \quad (\text{D11})$$

Inserting $a^* = \tilde{\Delta} + iJ\Delta/4$, the emission term becomes

$$\frac{1}{4} e^{ia^*t} I(t) = \frac{1}{4} \int_0^t dx C(t-x) e^{-\frac{J\tilde{\Delta}}{4}x} \frac{\sin(\tilde{\Delta}x)}{\tilde{\Delta}} \quad (\text{D12})$$

$$= \frac{1}{4} Z_a(t). \quad (\text{D13})$$

The net matrix element reads

$$\Phi_{21,12}(t) = \frac{1}{4} \left[Z_a(t) + e^{-J\Delta t/2} [Z_{-a}(t)]^* \right], \quad (\text{D14})$$

where we introduced the kernel

$$Z_{x+iy}(t) \equiv \int_0^t d\tau C(t-\tau) \frac{\sin(x\tau)}{x} e^{y\tau}. \quad (\text{D15})$$

The last two equations yield Eqs. (89) and (90), respectively.

b. Laplace representation

Next we evaluate the Laplace transform of Eq. (D14). The Laplace transform of the kernel is

$$\begin{aligned} \tilde{Z}_{x+iy}(s) &= \int_0^\infty Z_{x+iy}(t) e^{-st} \\ &= \frac{\tilde{C}(s)}{x^2 + (s-y)^2}. \end{aligned} \quad (\text{D16})$$

Hence,

$$\tilde{\Phi}_{21,12}(s) = \frac{1}{4} \frac{\tilde{C}(s) + [\tilde{C}(s^* + J\Delta/2)]^*}{(s + J\Delta/4)^2 + \tilde{\Delta}^2}. \quad (\text{D17})$$

In the Fourier–Laplace representation $s = -i\omega$ and $\tilde{C}(s) = \Gamma_\omega$,

$$\tilde{\Phi}_{21,12}(\omega) = -\frac{1}{4} \frac{\Gamma_\omega + [\Gamma_{-\omega^* + iJ\Delta/2}]^*}{(\omega + iJ\Delta/4)^2 - \tilde{\Delta}^2}. \quad (\text{D18})$$

Integrating along the Bromwich contour gives Eq. (91) of the main text,

$$\Phi_{21,12}(t) = -\frac{1}{8\pi} \int_{-\infty+i0^+}^{\infty+i0^+} d\omega e^{-i\omega t} \frac{\Gamma_\omega + [\Gamma_{-\omega^* + iJ\Delta/2}]^*}{(\omega + iJ\Delta/4)^2 - \tilde{\Delta}^2}. \quad (\text{D19})$$

The analytic structure of the integrand contains poles at $\omega = \pm\tilde{\Delta} - iJ\Delta/4$ together with a branch cut along the real axis. Accordingly the coherence separates into

$$\Phi_{21,12}(t) = \Phi^{\text{pole}}(t) + \Phi^{\text{cut}}(t). \quad (\text{D20})$$

c. Off-diagonal pole contribution

The pole contribution is obtained from the residues in the lower half plane at $\omega_\pm = \pm\tilde{\Delta} - iJ\Delta/4$. After straightforward algebra, this yields Eq. (92) of the main text:

$$\begin{aligned} \Phi_{21,12}^{\text{pole}}(t) &= \frac{i}{8\tilde{\Delta}} e^{-J\Delta t/4} \left[e^{-i\tilde{\Delta}t} (\Gamma_a + (\Gamma_{-a})^*) \right. \\ &\quad \left. - e^{+i\tilde{\Delta}t} (\Gamma_{-a^*} + (\Gamma_{a^*})^*) \right]. \end{aligned} \quad (\text{D21})$$

In the weak-coupling limit

$$a \rightarrow \Delta - i0^+,$$

the pole contribution reduces to Eq. (94) of the main text:

$$\Phi_{21,12}^{\text{pole}}(t) = -\frac{i}{4} e^{-J\Delta t/4} \frac{\cos(\tilde{\Delta}t)}{\tilde{\Delta}} (\Gamma_\Delta^* + \Gamma_{-\Delta}). \quad (\text{D22})$$

d. Off-diagonal branch-cut contribution

In the emission component (integrand proportional to $[\Gamma_{-\omega^* + iJ\Delta/2}]^*$ in Eq. (D19)), the change of variables $\omega \rightarrow -\omega$ puts the branch-cut contribution into the form

$$\begin{aligned} \Phi_{21,12}^{\text{cut}}(t) &= -\frac{1}{4\pi} \int_0^\infty d\omega \frac{e^{-i\omega t} J_\omega}{(\omega + iJ\Delta/4)^2 - \tilde{\Delta}^2} \\ &\quad - \frac{e^{-J\Delta t/2}}{4\pi} \int_0^\infty d\omega \frac{e^{+i\omega t} J_\omega}{(\omega + iJ\Delta/4)^2 - \tilde{\Delta}^2}. \end{aligned} \quad (\text{D23})$$

This yields Eq. (95) of the main text.

The two terms in Eq. (D23) correspond to the emission and absorption continua. These contributions behave differently. The emission branch cut produces an on-shell component that combines with the pole term and determines the pointer direction, whereas the absorption continuum contains no such on-shell contribution and contributes only to the remaining continuum correction.

We first analyze the emission continuum contribution

$$I(t) \equiv -\frac{1}{4\pi} \int_0^\infty d\omega \frac{e^{-i\omega t} J_\omega}{(\omega + iJ\Delta/4)^2 - \tilde{\Delta}^2}. \quad (\text{D24})$$

To evaluate $I(t)$ we deform the contour into the lower half plane. The integral then separates into an on-shell residue and a vertical contour contribution,

$$I(t) = I_{\text{shell}}(t) + I_{\text{vert}}(t). \quad (\text{D25})$$

The denominator has poles at

$$\omega_{\pm} = -\frac{iJ_{\Delta}}{4} \pm \tilde{\Delta}. \quad (\text{D26})$$

The pole in the fourth quadrant,

$$\omega_p = \tilde{\Delta} - \frac{iJ_{\Delta}}{4}, \quad (\text{D27})$$

gives the residue

$$I_{\text{shell}}(t) = \frac{i}{4\tilde{\Delta}} J_{\omega_p} e^{-i\omega_p t} = \frac{i}{4\tilde{\Delta}} J_{\omega_p} e^{-i\tilde{\Delta}t} e^{-J_{\Delta}t/4}. \quad (\text{D28})$$

This on-shell contribution arises solely from the emission branch cut and yields Eq. (96) of the main text. It combines with the pole term (D22) to produce

$$\Phi_{21,12}^{\text{pole+shell}}(t) = e^{-J_{\Delta}t/4} X(t), \quad (\text{D29})$$

where $X(t)$ is given in Eq. (98) of the main text.

The remaining terms arise from the continuum contributions. In contrast to the emission branch cut, the absorption continuum does not produce an on-shell component and therefore contributes only through the remaining vertical contour integral. The vertical segment is oriented from $-i\infty$ to 0. Writing

$$\omega = -iy, \quad y: \infty \rightarrow 0, \quad d\omega = -i dy, \quad (\text{D30})$$

one finds

$$\int_{-i\infty}^0 f(\omega) d\omega = i \int_0^{\infty} f(-iy) dy. \quad (\text{D31})$$

Since

$$(-iy + iJ_{\Delta}/4)^2 - \tilde{\Delta}^2 = -\left[\tilde{\Delta}^2 + (y - J_{\Delta}/4)^2\right], \quad (\text{D32})$$

and

$$J_{-iy} = 2\pi\lambda^2 \omega_c \left(\frac{-iy}{\omega_c}\right)^s e^{iy/\omega_c} = 2\pi\lambda^2 \omega_c^{1-s} y^s e^{-i\pi s/2} e^{iy/\omega_c}, \quad (\text{D33})$$

the vertical contribution becomes

$$I_{\text{vert}}(t) = -\frac{i\lambda^2 \omega_c^{1-s} e^{-i\pi s/2}}{2} \int_0^{\infty} dy \frac{y^s e^{-yt} e^{iy/\omega_c}}{\tilde{\Delta}^2 + (y - J_{\Delta}/4)^2}. \quad (\text{D34})$$

The exponential factor e^{-yt} restricts the dominant integration region to $y \sim t^{-1}$. For times $t \gg \tilde{\Delta}^{-1}, \omega_c^{-1}$ this implies $y \ll \tilde{\Delta}, \omega_c$ over the dominant region. The phase factor e^{iy/ω_c} and the denominator $\tilde{\Delta}^2 + (y - J_{\Delta}/4)^2$ may therefore be replaced, to leading order, by their endpoint values at $y = 0$. This gives

$$I_{\text{vert}}(t) \approx -\frac{i\lambda^2 \omega_c^{1-s} e^{-i\pi s/2}}{2(\tilde{\Delta}^2 + J_{\Delta}^2/16)} \int_0^{\infty} dy y^s e^{-yt}, \quad (\text{D35})$$

$$t \gg \tilde{\Delta}^{-1}, \omega_c^{-1}.$$

The remaining integral is elementary,

$$\int_0^{\infty} dy y^s e^{-yt} = \Gamma(s+1) t^{-(s+1)}, \quad (\text{D36})$$

and therefore

$$I_{\text{vert}}(t) \approx -\frac{i\lambda^2 \omega_c^{1-s} e^{-i\pi s/2}}{2} \frac{\Gamma(s+1)}{\tilde{\Delta}^2 + J_{\Delta}^2/16} t^{-(s+1)}. \quad (\text{D37})$$

Thus, inserting Eq. (13), the vertical contribution already exhibits the Khalfin tail for $t \gg \tilde{\Delta}^{-1}, \omega_c^{-1}$.

The absorption branch cut is treated similarly. Since it remains off shell, it produces no additional on-shell term and contributes only the analogous continuum piece,

$$\Phi_{21,12}^{\text{abs,cut}}(t) \sim e^{-J_{\Delta}t/2} \frac{C(t)^*}{4\tilde{\Delta}^2}. \quad (\text{D38})$$

It is therefore exponentially suppressed at late times, so that the asymptotic tail of the full branch-cut contribution is

$$\Phi_{21,12}^{\text{cut}}(t) \sim \frac{C(t)}{4\tilde{\Delta}^2}. \quad (\text{D39})$$

Collecting all contributions, the off-diagonal coherence dynamics therefore consists of an exponentially damped pole-plus-shell term that selects the pointer direction, together with a continuum correction whose asymptotic form is the Khalfin tail.

3. Population Dynamics

We first derive the disentangled population map to leading order in weak coupling and then determine its Wigner-Weisskopf asymptotics.

In the population sector the Davies reference generator

$$(L_0)_{\text{pop}} = \frac{J_{\Delta}}{2} \begin{pmatrix} -1 & 0 \\ 1 & 0 \end{pmatrix}, \quad (\text{D40})$$

with exponential

$$e^{(L_0)_{\text{pop}}t} = \begin{pmatrix} e^{-J_{\Delta}t/2} & 0 \\ 1 - e^{-J_{\Delta}t/2} & 1 \end{pmatrix}. \quad (\text{D41})$$

The resummed generator reads

$$L_{\text{pop}}(t) = \frac{1}{2} \text{Re} \begin{pmatrix} -\Gamma_+(t) & \Gamma_-(t) \\ \Gamma_+(t) & -\Gamma_-(t) \end{pmatrix}. \quad (\text{D42})$$

Inserting this into the disentanglement formula,

$$C_{\text{pop}}(t) = \int_0^t d\tau e^{(L_0)_{\text{pop}}(t-\tau)} [L_{\text{pop}}(\tau) - (L_0)_{\text{pop}}] e^{(L_0)_{\text{pop}}\tau}, \quad (\text{D43})$$

and noting that the exponential matrices are real, the real part may be taken outside the integral. One obtains

$$C_{\text{pop}}(t) = \begin{pmatrix} A(t) & B(t) \\ -A(t) & -B(t) \end{pmatrix}, \quad (\text{D44})$$

with

$$A(t) = \frac{J_{\Delta}t}{2} e^{-J_{\Delta}t/2} - \frac{e^{-J_{\Delta}t/2}}{2} \text{Re} \int_0^t d\tau \left[\Gamma_+(\tau) - (e^{J_{\Delta}\tau/2} - 1)\Gamma_-(\tau) \right] \quad (\text{D45})$$

$$B(t) = \frac{1}{2} \text{Re} \int_0^t d\tau e^{-J_{\Delta}(t-\tau)/2} \Gamma_-(\tau). \quad (\text{D46})$$

The disentangled population map therefore becomes

$$\Phi_{\text{pop}}(t) = \begin{pmatrix} e^{-J_{\Delta}t/2} + A(t) & B(t) \\ 1 - e^{-J_{\Delta}t/2} - A(t) & 1 - B(t) \end{pmatrix}. \quad (\text{D47})$$

The key point is that the apparent secular term in $A(t)$ is cancelled by the memory contribution, so that at Wigner–Weisskopf time scales the population sector reduces to the Davies semigroup plus an $O(\lambda^2)$ static correction.

To evaluate $B(t)$, we substitute

$$\Gamma_-(\tau) = \int_0^{\tau} ds C(s) e^{-ias}, \quad a = \tilde{\Delta} - iJ_{\Delta}/4, \quad (\text{D48})$$

into Eq. (D46). Interchanging the order of integration and performing the elementary τ -integration yields

$$B(t) = \frac{1}{J_{\Delta}} \text{Re} \int_0^t ds C(s) e^{-ias} \left(1 - e^{-J_{\Delta}(t-s)/2} \right). \quad (\text{D49})$$

Separating the two terms gives

$$B(t) = \frac{1}{J_{\Delta}} \text{Re} \left[\int_0^t ds C(s) e^{-ias} - e^{-J_{\Delta}t/2} \int_0^t ds C(s) e^{-i(a+iJ_{\Delta}/2)s} \right]. \quad (\text{D50})$$

Using the kernel introduced above,

$$\Gamma_z(t) \equiv \int_0^t d\tau C(\tau) e^{iz\tau}, \quad (\text{D51})$$

this becomes

$$B(t) = \frac{1}{J_{\Delta}} \text{Re} \left[\Gamma_{-a}(t) - e^{-J_{\Delta}t/2} \Gamma_{-(a+iJ_{\Delta}/2)}(t) \right]. \quad (\text{D52})$$

To evaluate $A(t)$, we write

$$A(t) = \frac{J_{\Delta}t}{2} e^{-J_{\Delta}t/2} - \frac{e^{-J_{\Delta}t/2}}{2} \text{Re} I_A(t), \quad (\text{D53})$$

where

$$I_A(t) \equiv \int_0^t d\tau \left[\Gamma_+(\tau) - (e^{J_{\Delta}\tau/2} - 1)\Gamma_-(\tau) \right]. \quad (\text{D54})$$

Using

$$\Gamma_{\pm}(\tau) = \int_0^{\tau} ds C(s) e^{\pm ias}, \quad a = \tilde{\Delta} - iJ_{\Delta}/4, \quad (\text{D55})$$

and exchanging the order of integration, the two contributions may be expressed in terms of the kernels

$$\Gamma_z(t) \equiv \int_0^t d\tau C(\tau) e^{iz\tau}, \quad \Sigma_z(t) \equiv \int_0^t d\tau \tau C(t-\tau) e^{-iz\tau}. \quad (\text{D56})$$

After straightforward algebra one obtains

$$I_A(t) = e^{iat} \Sigma_a(t) - \frac{2}{J_{\Delta}} e^{J_{\Delta}t/2} \Gamma_{-a}(t) + \frac{2}{J_{\Delta}} \Gamma_{-(a+iJ_{\Delta}/2)}(t) + e^{-iat} \Sigma_{-a}(t). \quad (\text{D57})$$

Using Eq. (D52), the final expression for $A(t)$ becomes

$$A(t) = \frac{J_{\Delta}t}{2} e^{-J_{\Delta}t/2} + B(t) - \frac{e^{-J_{\Delta}t/2}}{2} \text{Re} \left[e^{iat} \Sigma_a(t) + e^{-iat} \Sigma_{-a}(t) \right], \quad (\text{D58})$$

where

$$a = \tilde{\Delta} - iJ_{\Delta}/4. \quad (\text{D59})$$

Eqs. (D47), (D52), and (D58) give the disentangled population map prior to taking asymptotic limits.

4. Wigner–Weisskopf asymptotics of the population sector

At the Wigner–Weisskopf time scale $t \sim O(\lambda^{-2})$, only $O(\lambda^0)$ terms multiplying the reference exponential are retained. As in the coherence sector, the explicit linear term $(J_{\Delta}t/2)e^{-J_{\Delta}t/2}$ in Eq. (D58) is cancelled by the combined contribution of the pole and the on-shell component of the emission branch cut (see, e.g., Eq. (C32)). The intermediate steps follow the same procedure as in the RWA Laplace–transform analysis and are therefore not repeated here.

We now determine the asymptotic form of the population map by examining $A(t)$ in Eq. (D58). As in the coherence sector, the kernels $\Sigma_z(t)$ are decomposed into pole and branch-cut contributions,

$$\Sigma_z(t) = \Sigma_z^{\text{pole}}(t) + \Sigma_z^{\text{bc}}(t), \quad (\text{D60})$$

where

$$\Sigma_z^{\text{pole}}(t) = e^{-izt} \left[t \Gamma_z + i \partial_{\omega} \Gamma_{\omega} \Big|_z \right], \quad (\text{D61})$$

which is identical to Eq. (C25).

After the cancellation of the linear terms in Eqs. (D58) and D61, the remaining terms are exponentially decaying and $O(\lambda^2)$. The reference semigroup in Eq. (D41) therefore dominates, giving to leading order

$$A(t) = B(t). \quad (\text{D62})$$

The corresponding population dynamics therefore takes the form of an affine map on the population vector,

$$\Phi_{\text{pop}}(t) = \begin{pmatrix} e^{-J_{\Delta}t/2} & 0 \\ 1 - e^{-J_{\Delta}t/2} & 1 \end{pmatrix} + B(t) \begin{pmatrix} 1 & 1 \\ -1 & -1 \end{pmatrix}. \quad (\text{D63})$$

At long times the second term in Eq. (D52) vanishes, since its internal growth is overcompensated by the external factor $e^{-J_{\Delta}t/2}$. Therefore

$$B_{\infty} = \frac{1}{J_{\Delta}} \text{Re} \Gamma_{-a}. \quad (\text{D64})$$

Expanding Γ_{-a} about $-\Delta$ and using $\text{Re} \Gamma_{-\Delta} = 0$ at zero

temperature, one obtains

$$B_{\infty} = -\frac{1}{4} \partial_{\omega} S_{\omega} \Big|_{-\Delta}, \quad (\text{D65})$$

which is precisely the $O(\lambda^2)$ stationary excited-state population, in agreement with the mean-force Gibbs state.

For $t \rightarrow \infty$, the oscillatory part of $\Gamma_{-a}(t)$ is governed by the pole contribution, so $B(t)$ approaches B_{∞} exponentially fast. No branch-cut contribution survives in the population. Hence, Eq. (D63) reduces to the population map in Eq. (104) of the main text.

Together, these appendices show that the same disentanglement framework underlies all sectors of the dynamics, while the different analytic structures of the corresponding kernels determine whether the late-time behavior is purely exponential, affine, or Khalfin-tailed.

-
- [1] H.-P. Breuer and F. Petruccione, *The Theory of Open Quantum Systems* (Oxford University Press, Oxford, 2002).
- [2] S. Chaturvedi and F. Shibata, *Zeitschrift für Physik B Condensed Matter* **35**, 297 (1979).
- [3] N. Van Kampen, *Physica* **74**, 215 (1974).
- [4] N. Van Kampen, *Physica* **74**, 239 (1974).
- [5] E. Crowder, L. Lampert, G. Manchanda, B. Shoffeitt, S. Gadamsetty, Y. Pei, S. Chaudhary, and D. Davidović, *Phys. Rev. A* **109**, 052205 (2024).
- [6] L. Lampert, S. Gadamsetty, S. Chaudhary, Y. Pei, J. Chen, E. Crowder, and D. Davidović, *Physical Review A* **111**, 042214 (2025).
- [7] Ángel Rivas and S. F. Huelga, *Open Quantum Systems: An Introduction*, SpringerBriefs in Physics (Springer, Heidelberg, 2012).
- [8] L. A. Khalfin, *Sov. Phys. JETP* **6**, 1053 (1958).
- [9] A. Peres, *Annals of Physics* **129**, 33 (1980).
- [10] G. Amato, H.-P. Breuer, and B. Vacchini, *Physical Review A* **99**, 052120 (2019).
- [11] A. S. Trushechkin, *Proceedings of the Steklov Institute of Mathematics* **313**, 246 (2021).
- [12] D. Tupkary, A. Dhar, M. Kulkarni, and A. Purkayastha, *Physical Review A* **109**, 032205 (2024).
- [13] A. D’Abbruzzo, V. Giovannetti, and V. Cavina, *Phys. Rev. Lett.* **135**, 240401 (2025).
- [14] W.-M. Zhang, P.-Y. Lo, H.-N. Xiong, M. W.-Y. Tu, and F. Nori, *Physical review letters* **109**, 170402 (2012).
- [15] P. Kumar, K. P. Athulya, and S. Ghosh, *Phys. Rev. B* **113**, 045404 (2026).
- [16] C. Blumenfeld, *Modifying the time-convolutionless master equation via the moore-penrose pseudoinverse* (2025), arXiv:2511.02556 [quant-ph].
- [17] G. Kaplanek and C. Burgess, *Journal of High Energy Physics* **2020**, 1 (2020).
- [18] A. D’Abbruzzo, D. Farina, and V. Giovannetti, *Phys. Rev. X* **14**, 031010 (2024).
- [19] A. J. Leggett, S. Chakravarty, A. T. Dorsey, M. P. A. Fisher, A. Garg, and W. Zwerger, *Rev. Mod. Phys.* **59**, 1 (1987).
- [20] A. Nazir and G. Schaller, The reaction coordinate mapping in quantum thermodynamics, in *Thermodynamics in the Quantum Regime: Fundamental Aspects and New Directions*, edited by F. Binder, L. A. Correa, C. Gogolin, J. Anders, and G. Adesso (Springer International Publishing, Cham, 2018) pp. 551–577.
- [21] E. B. Davies, *Comm. Math. Phys.* **39**, 91 (1974).
- [22] D. Davidović, *Quantum* **4**, 326 (2020).
- [23] Similar use of a contractive semigroup as a leading reference evolution appears in rigorous weak-coupling approaches [36, 37]. In those works the semigroup approximates the exact reduced dynamics, whereas here it serves as the reference trajectory relative to which the dynamical map is reconstructed.
- [24] H.-P. Breuer and F. Petruccione, *The theory of open quantum systems* (Oxford University Press, Oxford, 2007).
- [25] C. Fleming, N. I. Cummings, C. Anastopoulos, and B. L. Hu, *Journal of Physics A: Mathematical and Theoretical* **43**, 405304 (2010).
- [26] R. Hartmann and W. T. Strunz, *Phys. Rev. A* **101**, 012103 (2020).
- [27] C. H. Fleming and N. I. Cummings, *Phys. Rev. E* **83**, 031117 (2011).
- [28] J. Thingna, J.-S. Wang, and P. Hänggi, *The Journal of Chemical Physics* **136**, 194110 (2012), <https://doi.org/10.1063/1.4718706>.
- [29] D. Tupkary, A. Dhar, M. Kulkarni, and A. Purkayastha, *Phys. Rev. A* **105**, 032208 (2022).
- [30] T. Becker, A. Schnell, and J. Thingna, *Phys. Rev. Lett.* **129**, 200403 (2022).
- [31] A. Strathearn, P. Kirton, D. Kilda, J. Keeling, and B. W. Lovett, *Nat. Commun.* **9**, 3322 (2018).
- [32] W. H. Zurek, *Reviews of Modern Physics* **75**, 715 (2003).
- [33] T. Forster, *Naturwissenschaften* **33**, 166 (1946).
- [34] N. Lorenzoni, T. Lacroix, J. Lim, D. Tamascelli, S. F. Huelga, and M. B. Plenio, *Science Advances* **11**, eady6751 (2025).
- [35] K. Nestmann and C. Timm, *Time-convolutionless master equation: Perturbative expansions to arbitrary order and*

application to quantum dots (2019), arXiv:1903.05132
[cond-mat.mes-hall].

[36] W. De Roeck and A. Kupiainen, in *Annales Henri*

Poincaré, Vol. 14 (Springer, 2013) pp. 253–311.

[37] M. Merkli, *Quantum* **6**, 615 (2022).